



# รายงานวิจัยฉบับสมบูรณ์

โครงการ การสังเคราะห์อนุภาคนาโนซิลิกาที่มีรูพรุน ที่มีคุณสมบัติไม่ชอบน้ำและน้ำมัน

โดย ดร. สิริญญา จันทรักษ์

ชันวาคม 2560

# สัญญาเลขที่ TRG5880154

# รายงานวิจัยฉบับสมบูรณ์

โครงการ การสังเคราะห์อนุภาคนาโนซิลิกาที่มีรูพรุน ที่มีคุณสมบัติไม่ชอบน้ำและน้ำมัน

ดร. สิริญญา จันทรักษ์ คณะวิทยาศาสตร์ มหาวิทยาลัยสงขลานครินทร์

สนับสนุนโดยสำนักงานกองทุนสนับสนุนการวิจัยและ มหาวิทยาลัยสงขลานครินทร์

(ความเห็นในรายงานนี้เป็นของผู้วิจัย สกว.และต้นสังกัดไม่จำเป็นต้องเห็นด้วยเสมอไป)

## **TABLE OF CONTENTS**

List of table	İ
List of figure	ii
Abstract	1
Introduction to the research problem and its significance	2
Literature review	5
Formation of surface roughness	5
Mesoporous nanoparticles	7
Objectives	9
Methodology	9
Synthesis of mesoporous silica nanoparticles using emulsion polymerization	9
Functionalization of mesoporous silica nanoparticles	10
Surface coating with mesoporous nanoparticles	11
Results and Discussion	11
Synthesis of mesoporous silica nanoparticles using emulsion polymerization	11
Functionalization of mesoporous silica nanoparticles	18
Surface coating with mesoporous nanoparticles	28
Conclusion	30
References	31
Appendix	34

## LIST OF TABLE

Table 1	Comparison of surface tension and contact angles of variable oils	4
	on smooth and rough surfaces	
Table 2	Synthesis condition of mesoporous silica nanoparticles using polystyrene	12
	template at varied TEOS:NH <sub>4</sub> OH ratio	
Table 3	Synthesis condition of size of mesoporous silica nanoparticles using	12
	polystyrene template at varied styrene concentration	
Table 4	Synthesis condition of size of mesoporous silica nanoparticles using	13
	polystyrene template at different amount of oil	
Table 5	Synthesis condition of size of mesoporous silica nanoparticles using	15
	poly(methyl methacrylate) template at varied methyl methacrylate concentration	
Table 6	Synthesis condition of size of mesoporous silica nanoparticles using CTAB	16
	template at varied ethanol concentration	
Table 7	Synthesis condition of mesoporous silica nanoparticles functionalized with	18
	trimethyl(trifluoromethylsilane) (F3) at varied TEOS:F-Silane ratio	
Table 8	Synthesis condition of mesoporous silica nanoparticles functionalized with	22
	trimethyl(trifluoromethylsilane) (F3) and trichloro(1H,1H,2H,2H-perfluorooctyl)	
	silane (F13) at varied TEOS:F-Silane ratio	
Table 9	Water contact angles of glass substrates coated with mesoporous silica	28
	nanoparticles functionalized with trimethyl(trifluoromethylsilane) (F3) at varied	
	TEOS: F-Silane ratio	
Table 1	0 Water contact angles of glass substrates coated with mesoporous silica	30
	nanoparticles functionalized with trimethyl(trifluoromethylsilane) (F3) and	
	trichloro-(1H,1H,2H,2H-perfluorooctyl)silane (F13) at varied TEOS:F-Silane ratio	

## LIST OF FIGURE

Figure 1 Schematic of contact angle measurement	2
Figure 2 Illustration of fluoroalkylsilane functionalized poly(vinyl alcohol) substrate	3
Figure 3 Images of water droplets on (a) fluorinate-coated glass and	3
(b) SiO <sub>2</sub> sphere arrays	
Figure 4 Wetting diagram described by Wenzel and Cassie-Baxter models	4
Figure 5 AFM (a) and SEM (b) – (d) images of surfaces after two-stage	5
roughening process	
Figure 6 Dependence of water contact angle on the size of SiO <sub>2</sub> particles	6
Figure 7 Diagram of aerosol reactor and mesoporous silica particles	7
Figure 8 SEM images of porous silica particles after removal of polystyrene	8
latex phase	
Figure 9 SEM (a) – (c) and TEM (d) images of porous silica particles synthesized	8
from CaCO <sub>3</sub> porous particles as solid templates	
Figure 10 Illustration shows mesoporous nanoparticle synthesized from emulsion	10
polymerization	
Figure 11 Illustration shows surface functionalization of mesoporous silica nanoparticle	11
Figure 12 SEM micrographs of mesoporous silica nanoparticles synthesized with	12
different TEOS:NH <sub>4</sub> OH volume ratios (a) 1:1, (b) 1:2, and (c) 1:3	
Figure 13 SEM micrographs of mesoporous silica nanoparticles synthesized with	13
different Styrene:TEOS volume ratios (a) 0.5:1, (b) 1:1, (c) 1.5:1, and (d) 2:1	
Figure 14 SEM micrographs of mesoporous silica nanoparticles synthesized at	14
different amount of oil (a) 6 mL and (b) 8 mL	
Figure 15 FT-IR spectrum of mesoporous silica nanoparticles before and after	14
template removal	

Figure 16 TEM images of mesoporous silica nanoparticles synthesized with different	15
Styrene:TEOS volume ratios (a) 0.5:1, (b) 1:1, (c) 1.5:1, and (d) 2:1	
Figure 17 SEM micrographs of mesoporous silica nanoparticles synthesized with	16
different MMA:TEOS volume ratios (a) 1:1 and (b) 2:1	
Figure 18 SEM and TEM micrographs of mesoporous silica nanoparticles synthesized	18
with different H2O:EtOH volume ratios (a-b) 150:50, (c-d) 160:40, (e-f) 170:30,	
(g-h) 180:20, and (i-j) 190:0	
Figure 19 TEM and SEM micrographs of mesoporous silica nanoparticles functionalized	19
with trimethyl(trifluoromethylsilane) (F3) at varied TEOS:F-Silane ratio (a-b) 5:1,	
(c) 3:1, and (d) 1:1	
Figure 20 FT-IR spectrum of mesoporous silica nanoparticles functionalized with	20
trimethyl(trifluoromethylsilane) (F3) at varied TEOS:F-Silane ratio	
Figure 21 SEM-EDS spectroscopic mapping of mesoporous silica nanoparticles	21
functionalized with trimethyl(trifluoromethylsilane) (F3) at varied TEOS:F-Silane	
ratio (a-b) 5:1, (c-d) 3:1, and (e-f) 1:1	
Figure 22 TGA thermograms of mesoporous silica nanoparticles functionalized with	21
trimethyl(trifluoromethylsilane) (F3) at varied TEOS:F-Silane ratio	
Figure 23 Nitrogen adsorption-desorption isotherms (a) (offset vertically by 500) and	22
BJH pore size distribution curves (b) of mesoporous silica nanoparticles	
functionalized with trimethyl(trifluoromethylsilane) (F3)	
Figure 24 SEM and TEM micrographs of mesoporous silica functionalized with	24
trimethyl(trifluoromethylsilane) (F3, a-f) and trichloro(1H,1H,2H,2H-perfluorooctyl)	
silane (F13, g-l) at varied TEOS:F-Silane ratio (a-b) F3-20:1, (c-d) F3-10:1,	
(e-f) F3-5:1, (g-h) F13-20:1, (i-j) F13-10:1, and (k-l) F13-5:1	

- Figure 25 SEM-EDS spectroscopic mapping of mesoporous silica nanoparticles

  functionalized with trichloro(1H,1H,2H,2H-perfluorooctyl)silane (F13) at varied

  TEOS:F-Silane ratio (a-b) 20:1, (c-d) 10:1, and (e-f) 5:1
- Figure 26 High resolution SEM micrographs of (a) bare mesoporous silica nanoparticles, 26

  (b) mesoporous silica nanoparticles functionalized with trimethyl(trifluoromethylsilane) (F3-5:1), and (c) mesoporous silica nanoparticles functionalized with trichloro(1H,1H,2H,2H-perfluorooctyl)silane (F13-5:1)
- Figure 27 TGA thermograms of mesoporous silica nanoparticles functionalized with

  27

  trichloro(1H,1H,2H,2H-perfluorooctyl)silane (F13) at varied TEOS:F-Silane ratio
- Figure 28 Nitrogen adsorption-desorption isotherms (a) (offset vertically by 200 and 700 27 for MSNP-4 and MSNP-F13-5,1, respectively) and BJH pore size distribution curves (b) of MSNPs
- Figure 29 AFM images of glass substrates coated with mesoporous silica nanoparticles 28 functionalized with trimethyl(trifluoromethylsilane) (F3) at TEOS:F-Silane ratio 5:1
- Figure 30 Photographs of water droplets on glass substrates coated with mesoporous

  silica nanoparticles functionalized with trimethyl(trifluoromethylsilane) (F3) at

  varied TEOS:F-Silane ratio (a) 1:0, (b) 5:1, (c) 3:1, and (d) 1:1
- Figure 31 Photographs of water droplets on glass substrates coated with mesoporous 30 silica nanoparticles functionalized with trimethyl(trifluoromethylsilane) (F3, a-c) and trichloro(1H,1H,2H,2H-perfluorooctyl)silane (F13, d-f) at varied TEOS:F-Silane ratio (a,d) 20:1, (b,e) 10:1, and (c,f) 5:1

เอกสารแนบหมายเลข 2

**Abstract** 

Project Code: TRG5880154

Project Title: A Novel Route to Synthesize Ultra-Oleophobic Mesoporous Silica

**Nanoparticles** 

Investigator: Dr. Sirinya Chantarak

Department of Materials Science and Technology

Faculty of Science, Prince of Songkla University

E-mail Address: sirinya.c@psu.ac.th

Project Period: 2 years

Mesoporous silica nanoparticles (MSNPs) have been used in variety of applications due to their morphology and porous structure. This work reports the one-pot synthesis of ultrahydrophobic MSNPs using N-cetyl-n,n,n-trimethyl ammonium bromide as a cationic surfactant template and ethanol (EtOH) as a cosolvent to form mesopores in the MSNPs. The effects of EtOH on the size and the pore structure of the MSNPs were studied by scanning electron microscopy and transmission electron microscopy. The results show that an addition of EtOH led to an enlargement of the MSNPs and a change in pore structure from a lamellar structure to a radially oriented structure. Cocondensation with two different types of fluoroalkyl silanes; trimethyl(fluoromethyl)silane, and trichloro(1H,1H,2H,2H-perfluorooctyl)silane provided low surface energy MSNPs with a core-shell structure. An assembly on the surface of these F-MSNPs generated nanostructure surface roughness rendering an improvement in surface wettability with water contact angle of 158.6°, which is a characteristic of oleophobic and ultrahydrophobic material.

Keywords: Silica nanoparticle; Core-shell; Porous material; Hydrophobic; Self-assembly

1

### Introduction to the research problem and its significance

During the past few years, touch-screen technologies have been developed rapidly to enable a variety of devices including tablet computers, smart phones, and automatic navigation systems. One of the crucial problems of a touch-screen display is the remaining of fingerprints that hinders clarity and reducing sensitivity of the screen. These fingerprints are evidence of human secretion containing triglycerides, wax monoesters, and fatty acids.<sup>1</sup>

To characterize anti-fingerprint properties of the surface, contact angles of water and *n*-hexadecane droplets are measured giving hydrophobicity and oleophobicity of the surface, respectively. The contact angle is calculated from Young's equation as shown in **Figure 1** and equation (a).

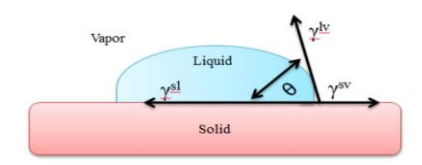


Figure 1. Schematic of contact angle measurement<sup>2</sup>

$$V^{sv} = V^{sl} + V^{lv} \cos \vartheta \qquad ----- (a)$$

 $\vartheta$  is the contact angle,  $\gamma^{s'}$  is the solid/liquid interfacial free energy,  $\gamma^{s'}$  is the solid surface free energy, and  $\gamma^{t'}$  is the liquid surface free energy.

Wu et al. reported results of human fingerprint tests that the surface is free from fingerprint traces when the contact angle is greater than 88°. Typically, hydrophobic surfaces have a contact angle above 95°, whereas oleophobic surfaces have a higher contact angle in the range of 105-120°. For super-hydrophobic surfaces, a water contact angle is greater than 150° with a sliding angle of water droplet less than 5°. 5

Several research groups have been focusing on mimicking surface morphology to lotus leaf, *Nelumbo nucifera*, in order to enhance hydrophobicity of the surface.<sup>6</sup> A combination of surface chemistry and roughness provides super hydrophobic property of the surfaces. However, this type of surface fails to repel oils or any liquids with low surface tension such as octane ( $\gamma^{\mu}$  = 21.6 mN/m), decane ( $\gamma^{\mu}$  = 23.8 mN/m), and hexadecane ( $\gamma^{\mu}$  = 27.5 mN/m). Such oils easily spread rapidly across the surfaces with

a contact angle of  $0^{\circ}$ .<sup>7,8</sup> In typical, the surface energies of water and oil are 72 mN/m and  $\sim$  20 to 40 mN/m, respectively.<sup>1</sup> To prepare fingerprint-free substrates, an oleophobic treatment is required to obtain a surface energy less than 20 mN/m.

Fluoroalkyl compounds are common chemicals with low surface energies, 10 – 15 mJ/m<sup>2</sup>. Chemical surface treatment with these compounds generates a fluorocarbon based thin-film providing oleophobic characteristic, as shown in **Figure 2**.

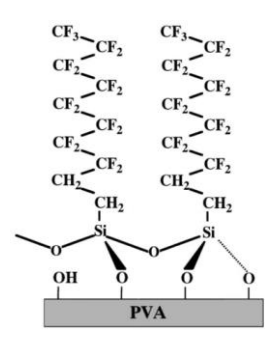


Figure 2. Illustration of fluoroalkylsilane functionalized poly(vinyl alcohol) substrate9

The surface coating with fluoroalkyl thin film is simply achieved by immersion of a substrate containing hydroxyl groups into a fluorinated silane solution. This method improve the water contact angle not greater than 125° while the roughness of the substrate is preserved as confirmed by AFM. Surface roughening has reported to increase the water contact angle since it is strongly influenced by the geometry, as shown in **Figure 3** and **Table 1**. In order to perform super-hydrophobic and oleophobic characteristics, the contact angle of water droplet needs to be greater than 150°.

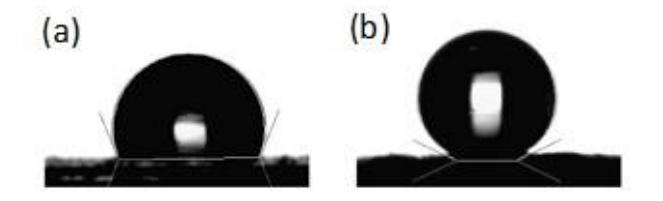


Figure 3. Images of water droplets on (a) fluorinate-coated glass and

(b) SiO<sub>2</sub> sphere arrays<sup>10</sup>

**Table 1.** Comparison of surface tension and contact angles of variable oils on smooth and rough surfaces<sup>11,12</sup>

		smo	oth sur	faces	rou	gh surf	aces			contact a	ngle/deg	
	γ (mN	$\theta_{\Lambda}$	$\theta_R$	$\Delta\theta$	$\theta_{\Lambda}$	$\theta_{R}$	$\Delta\theta$	_	wa	ter	de	cane
	$m^{-1}$ )	(deg)	(deg)	(deg)	(deg)	(deg)	(deg)	treatment	flat	porous	flat	porous
water	72.0	113	99	14	161	155	6	untreated	$116 \pm 2$	$146 \pm 1$	46 ± 2	wicks
ethylene glycol	48.0	86	68	18	128	118	10	O <sub>2</sub> plasma plasma polymer	$131 \pm 4$ $131 \pm 3$	$153 \pm 2$ $144 \pm 1$	$55 \pm 2$ $83 \pm 1$	wicks $115 \pm 1$
hexadecane	27.5	66	51	15	120	109	11	O <sub>2</sub> plasma + plasma polymer	$148 \pm 1$	$152 \pm 1$	$92 \pm 3$	$133 \pm 2$
dodecane	25.3	63	50	13	105	95	10					
decane	23.8	56	42	14	94	85	9					
octane	21.6	55	43	12	85	74	11					
heptane	20.1	41	35	6	76	65	11					
hexane	18.4	39	34	5	71	60	11					

Wenzel and Cassie-Baxter are two theories used to describe the wettability of a surface, as shown in **Figure 4**. <sup>13,14</sup> The former assumes that the liquid completely wets the flat surface, whereas the later assumes that the liquid rests on the peaks of the rough structures. The rough surfaces exhibit hydrophobic and oleophobic properties due to trapped air within the voids of the texture. These voids repel the liquid from fully wetting the composite surface. <sup>8,15,16</sup>

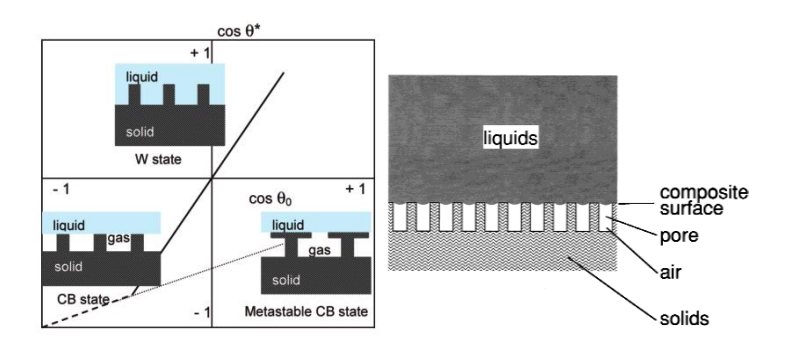


Figure 4. Wetting diagram described by Wenzel and Cassie-Baxter models 11,17

However, the surface modification by surface roughening and chemical treatment results in reduction of the optical transparency of the substrates. The drawback of these techniques is not suitable for anti-fingerprint applications of the touch-screen technologies. The goal of this research is to develop coating materials that can provide super hydrophobic, super oleophobic properties with high transparency.

#### Literature review

#### Formation of surface roughness

Several techniques have been reported to generate nano-scale surface roughness that maintains the optical transparency over 90% in the region of visible light. Tadanaga et al. prepared nano-pores on hydrophobic alumina films by boiling alumina sheets in water generating flowerlike structures that rendered super-water-repellent behavior with a contact angle of 165°. 17,18 Irregular topography in nanoscale produced from recrystallization of polymer solutions on substrates was reported by Erbil et al. and Onda et al. to perform a water contact angle as high as 174°. 19,20 Evaporation of a polymer solution under humid conditions was reported Yabu and Shimomura to yield a honeycomb-like surface with tunable pore size by controlling the humidity and the size of water droplets on the wet film.<sup>6</sup> Si substrates etched by photolithography with combination of chemical etching and deep reactive ion etching was also reported by Tuteja et al. and Cao et al. to provide super-hydrophobicity. Two-stage surface roughening of substrate such as nanopillar structures on micro-roughening surface was reported to exhibit super-hydrophobic and ultra-oleophobic properties with an oil contact angle over 100°, as shown in Figure 5.21,22,23 However, all the techniques that have been mentioned above require sophisticated equipment, high cost of processing, and have limitation on exposed surface area which is not suitable for industrial scale.

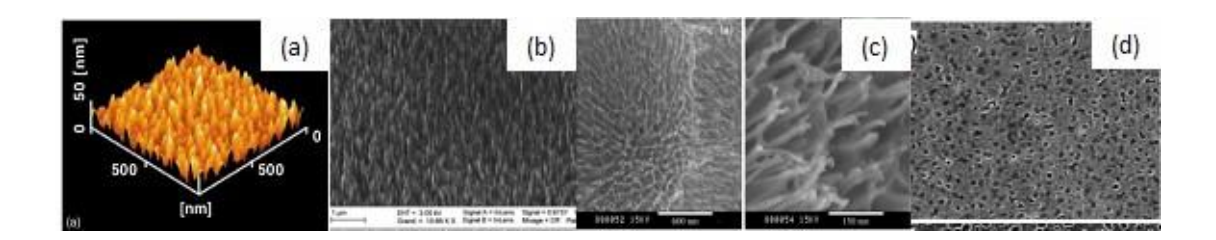


Figure 5. AFM (a) and SEM (b) – (d) images of surfaces after two-stage roughening process<sup>21,22,23</sup>

Layer-by-layer assembly of nanoparticles is another method that has been reported to create surface roughness at relatively low cost and on large scale. A crucial limitation of this technique is that the size of particles and the thickness of the assemble

nanoparticle layer have to be controlled in order to maintain the optical transparency of the substrates. 1,8,15,24,25-26

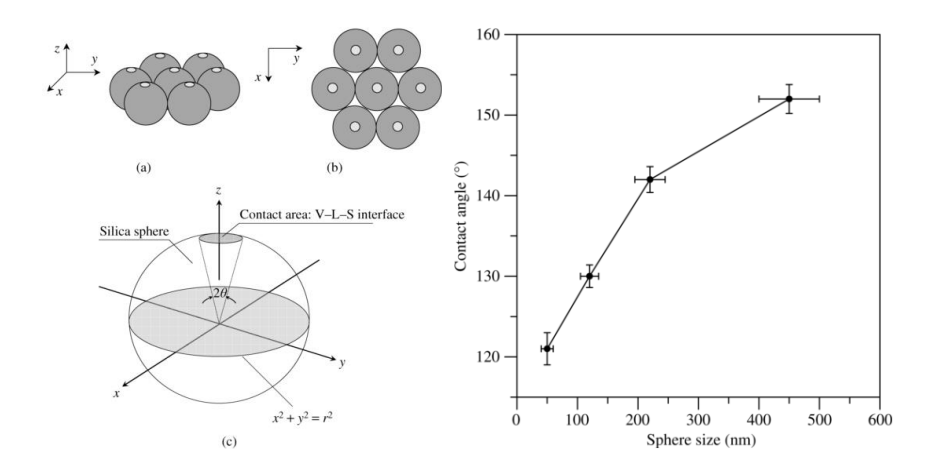


Figure 6. Dependence of water contact angle on the size of SiO<sub>2</sub> particles<sup>10</sup>

Altering the size of the particles affects surface topography and water contact angles, as shown in **Figure 6**. The contact angle of water is significantly affected by the size of the particles on the surface due to the size of cavities or surface roughness generated from the assembly of the particles. The difference in diameter of particles provides different a contact area to the water droplet as explained by Wenzel model, and different size of voids for air trapping explained by Cassie model. These are the important factors that improve the hydrophobic and oleophobic properties of the surfaces. In the case of Cassie-Baxter's theory,  $\varphi_s$  is calculated from equation (b) as shown below

$$\varphi_s = \frac{S_c}{S_p} = \frac{\sum_{i=1}^n S_{ci}}{S_p} \qquad ----- (b)$$

where  $S_p$  is projected area and  $S_c$  is contact area of the water droplet, respectively. Closed-packing assembly of large particles provides a large cavity for air-trapping, and high surface curvature which increases a floating force against the liquid droplet at the interface.<sup>10</sup>

#### Mesoporous nanoparticles

Recently, only a few methods were reported for preparation of mesoporous nanoparticles. The first method is aerosol-based processing where structures within the particles can be created to hexagonal, cubic, or vesicular morphologies by controlling the evaporation rate and interfacial-induced self-assembly of the aerosol droplets within the heating chamber, **Figure 7**.<sup>27,28</sup> Although this method can provide variable internal structures of the particles, it requires a complicated equipment which contains atomizer and drying tube with different heating temperatures.

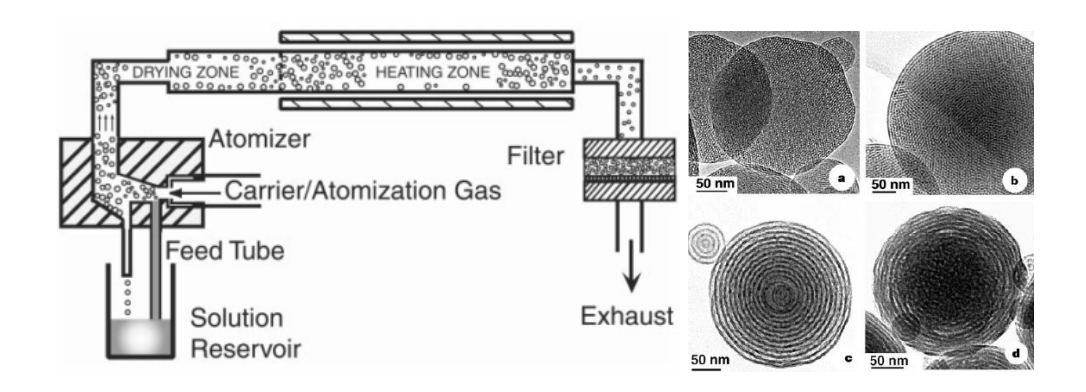
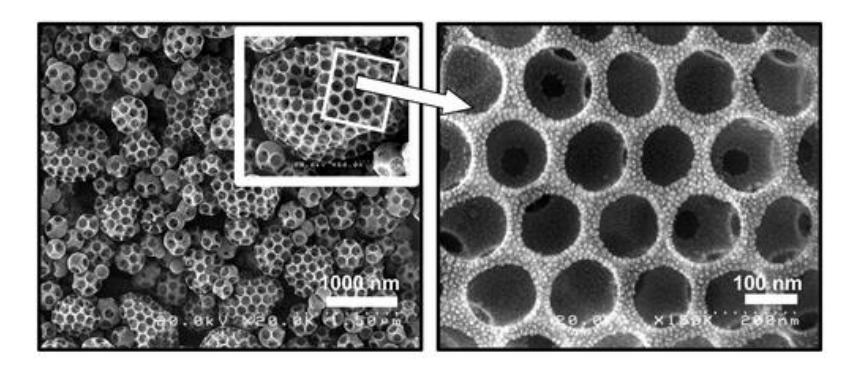


Figure 7. Diagram of aerosol reactor and mesoporous silica particles<sup>27</sup>

The Second method is spray drying of solution containing two types of particles. Iskanda *et al.* prepared porous silica particles from mix solution of silica and polystyrene latex colloids. This co-solution was atomized to form micrometer-sized droplets. The droplets were transferred to a drying reactor with different heating zones to evaporate solvent, decompose styrene phase, and cure the silica phase. Porous silica particles with hexagonal packing of particles, **Figure 8**, were obtained after passing through this equipment.<sup>29</sup>



**Figure 8**. SEM images of porous silica particles after removal of polystyrene latex phase<sup>29</sup>

The third method is synthesis of particles using template. Mao *et al.* reported synthesis of porous silica microspheres using sol-gel process in the presence of CaCO<sub>3</sub> porous particles as solid templates.<sup>30</sup> The template was further removed by dissolution with hydrochloric acid after polymerization resulting in porous silica particles, **Figure 9**.

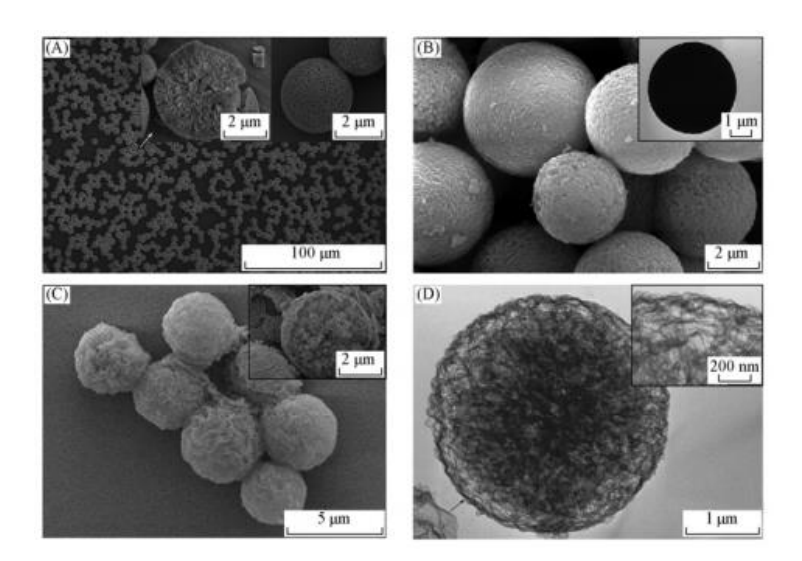


Figure 9. SEM (a) - (c) and TEM (d) images of porous silica particles synthesized from  $CaCO_3$  porous particles as solid templates<sup>30</sup>

The goal of this work is to prepare ultra oleophobic and super hydrophobic surfaces by generating dual morphology of surface roughness using mesoporous nanoparticles. The diameter of the assemble nanoparticles will control a contact area to water droplet, whereas the pore size will control amount of trapped air within the voids. From the literatures mentioned previously, the mesoporous particles were prepared from

methods that required sophisticated or special-built instrument, which is not a costeffective technique for industrial scale. Moreover, calcination at extremely high temperature is needed which is an energy consumption process.

#### **Objectives**

- 1. To develop a novel route that is simple and cost-effective for synthesis of mesoporous silica nanoparticles
- To develop surface coating technique using mesoporous silica nanoparticles as coating material that provides super hydrophobic and ultra oleophobic properties with high transparency
- 3. To perform a pilot study of using mesoporous silica nanoparticles in controlled drug release applications

#### Methodology

### Synthesis of mesoporous silica nanoparticles using emulsion polymerization

Surface roughening was reported to increase hydrophobicity of the surface, however, the transparency of the substrate decreases due to Mie scattering. The challenge of this research is to create rough features performing ultra oleophobicity and super hydrophobicity while the optical transparency of the substrates is maintained. In this research, a simple and low-cost method (*i.e.* control assembly of mesoporous silica nanoparticles, as coating materials) was conducted to generate dual morphology of the surface roughness.

The mesoporous silica nanoparticles were synthesized using an organic water/oil mixture.<sup>33</sup> Briefly, template method in а surfactant cetyltrimethylammonium bromide (CTAB) or sodium dodecyl sulfate (SDS), were used to form micelles in water/oil solution. The size of micelles was varied depending on type of surfactant. After the step of micelle formation, hydrolytic condensation of tetraethylorthosilicate (TEOS, silica monomer) and co-monomer such as styrene monomer or methyl methacrylate monomer was added. These two types of monomer were trapped inside the micelles forming co-monomer droplets. The polymerization was proceeded by addition of initiator yielding composite of silica/polystyrene (PS) or silica/poly(methyl methacrylate) (PMMA) nanoparticles. Removal of polymer phase was reported by several research groups using calcination at high temperatures, typically

greater than 500°C, inside sophisticated instrument. However, the aim of this work is to develop the technique that is simple, low cost, and doable with simple apparatus for a large scale. Therefore, the co-polymer phase, *i.e.* PS or PMMA, was removed using chemical treatment or dissolution in a specific solvent such as toluene, tetrahydrofuran, or dilute hydrochloric acid to obtain the mesoporous silica nanoparticles, as shown in **Figure 10**. The solvent after template removal can be re-purified by simple distillation and re-use within the process. With this technique, the chemical structure of the surfactant, pH of solution, ionic strength of surfactant molecules, temperature of synthesis, monomer/co-monomer ratio, were crucial factors that controlled the size of the nanoparticles. The size and structure of mesoporous nanoparticles before and after removal of template were characterized using Scanning Electron Microscopy (SEM) and Transmission Electron Microscopy TEM).

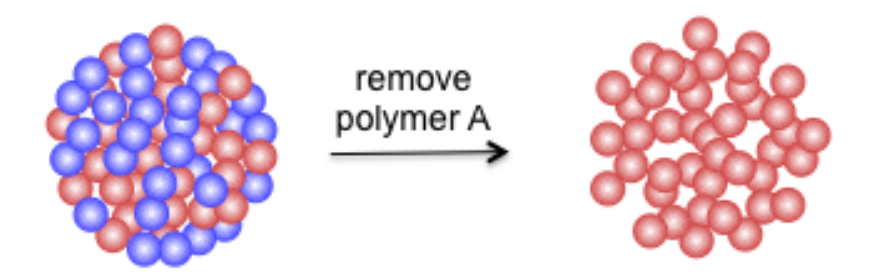


**Figure 10.** Illustration shows mesoporous nanoparticle synthesized from emulsion polymerization

#### Functionalization of mesoporous silica nanoparticles

To achieve super hydrophobic and ultra oleophobic surface, post chemical functionalization with fluorinated silanes was performed. The fluorinated silanes provide low surface energy, typically less than 20 mJ/m², to water contact angle that leads to anti-wettability surfaces. In this work, the mesoporous silica nanoparticles after template removal were functionalized with fluorinated silane to enhance the hydrophobicity and oleophobicity of porous surfaces.<sup>5,24,31</sup> The process of fluorinated functionalization of silica nanoparticles was approached by co-polymerization of silanes or post chemical modification to the surfaces by formation of fluorinated thin film, **Figure 11**. The thickness of fluorinated thin film and type of fluoroalkyl silane were studied to optimize surface properties in both hydrophobicity and transparency. The mesoporous silica nanoparticles were characterized before and after functionalization with fluorinated silanes using Fourier-Transform Infrared Spectroscopy (FT-IR). The porosity of the

nanoparticles was examined by using Brunauer-Emmett-Teller (BET) method and the pore size was obtained from Barrett-Joyner-Halenda (BJH) method.

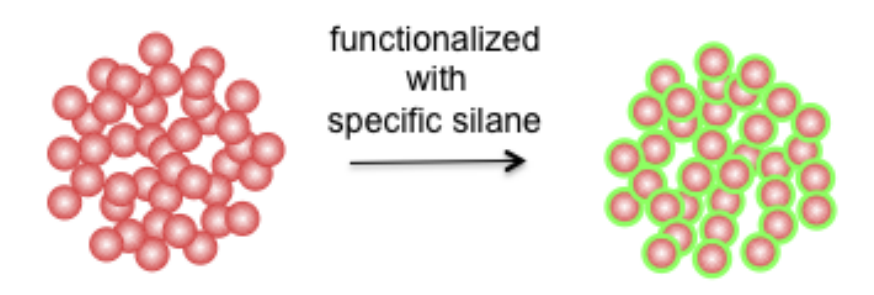


Figure 11. Illustration shows surface functionalization of mesoporous silica nanoparticle

#### Surface coating with mesoporous nanoparticles

The mesoporous silica nanoparticles with controlled shape and size in the range of 5 – 200 nm and the pore size in the range of 5 – 50 nm were homogeneously coated on transparent substrates such as glass using spin coating technique to form dual morphologies or double roughness. This technique rendered assemblies of mesoporous silica nanoparticle, leading to variation in transparency of modified substrates. Contact Angle measurement (CA) was performed to study hydrophobicity of the surface with water droplet and oleophobicity of the substrate with oil droplet. Atomic Force Microscopy (AFM) and SEM were utilized to investigate topography and morphology of the substrate after surface coating.

#### **Results and Discussion**

# Synthesis of mesoporous silica nanoparticles using emulsion polymerization

Polymer Template

Effect of pH of the solution on the size of mesoporous silica nanoparticles was studied. By varying the amount of ammonium hydroxide (NH<sub>4</sub>OH) solution, it can be seen that increasing the amount of NH<sub>4</sub>OH led to an enlargement of mesoporous silica nanoparticles, **Table 2**. However, size distribution of the mesoporous silica nanoparticles was broader and the shape of the nanoparticles was spherical-like as shown in **Figure 12**.

**Table 2.** Synthesis condition of mesoporous silica nanoparticles using polystyrene template at varied TEOS:NH<sub>4</sub>OH ratio

Sample	Water	Octane	Styrene	TEOS	NH₄OH	Size
	(mL)	(mL)	(mL)	(mL)	(mL)	(nm)
Sample – 1	30	8	1.0	1.0	1.2	122±19
Sample – 2	30	8	1.0	1.0	2.4	151±30
Sample – 3	30	8	1.0	1.0	3.6	196±43

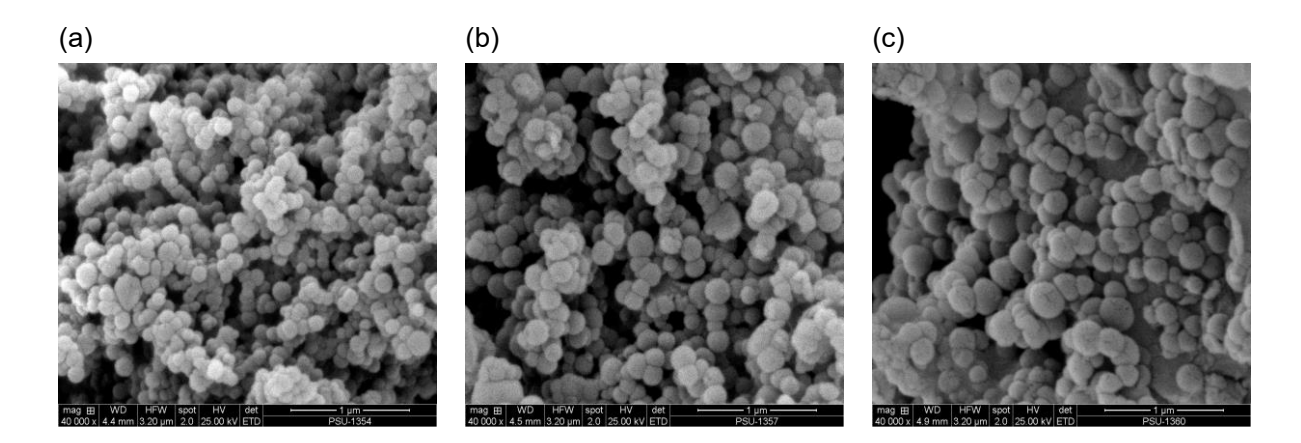


**Figure 12.** SEM micrographs of mesoporous silica nanoparticles synthesized with different TEOS:NH<sub>4</sub>OH volume ratios (a) 1:1, (b) 1:2, and (c) 1:3

Effect of styrene concentration on the size of mesoporous silica nanoparticles was studied. By varying the amount of styrene monomer, it can be seen that increasing the amount of styrene monomer led to an enlargement of mesoporous silica nanoparticles, **Table 3**. However, the shape of the nanoparticles was distorted as shown in **Figure 13**.

**Table 3.** Synthesis condition of size of mesoporous silica nanoparticles using polystyrene template at varied styrene concentration

Sample	Water	Octane	Styrene	TEOS	NH₄OH	Size
	(mL)	(mL)	(mL)	(mL)	(mL)	(nm)
Sample – 4	30	8	0.5	1.0	1.2	100±13
Sample – 5	30	8	1.0	1.0	1.2	100±15
Sample – 6	30	8	1.5	1.0	1.2	128±22
Sample – 7	30	8	2.0	1.0	1.2	117±18

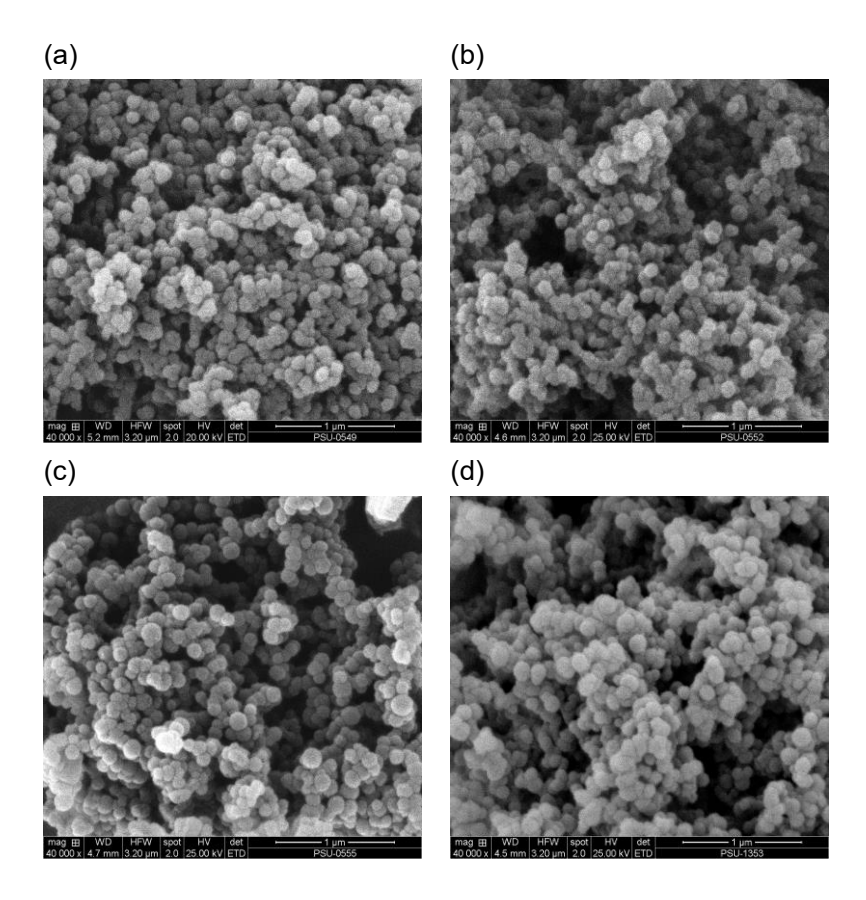


**Figure 13.** SEM micrographs of mesoporous silica nanoparticles synthesized with different Styrene:TEOS volume ratios (a) 0.5:1, (b) 1:1, (c) 1.5:1, and (d) 2:1

Effect of size of oil droplet on the size of mesoporous silica nanoparticles was studied. By varying the amount of octane, it can be seen that increasing the amount of octane led to an enlargement of mesoporous silica nanoparticles, **Table 4**. However, However, the shape of the nanoparticles was distorted as shown in **Figure 14**.

**Table 4.** Synthesis condition of size of mesoporous silica nanoparticles using polystyrene template at different amount of oil

Sample	Water	Octane	Styrene	TEOS	NH₄OH	Size
	(mL)	(mL)	(mL)	(mL)	(mL)	(nm)
Sample – 8	30	6	2.0	1.0	1.2	89±11
Sample – 9	30	8	2.0	1.0	1.2	117±18

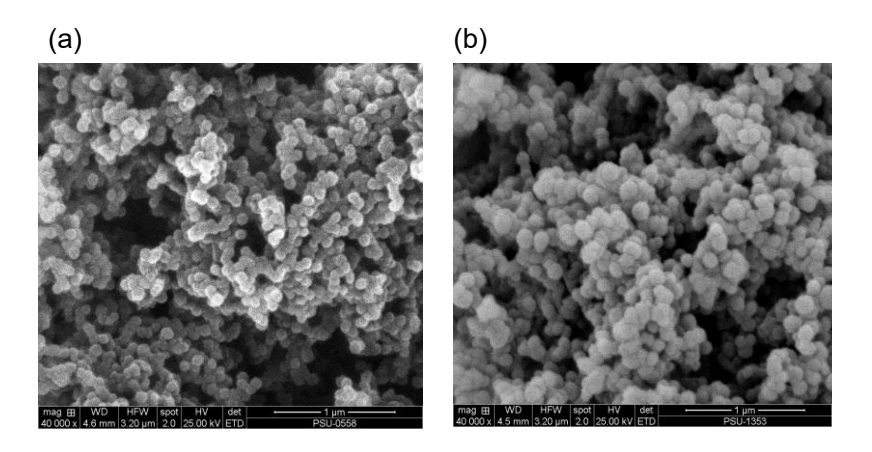
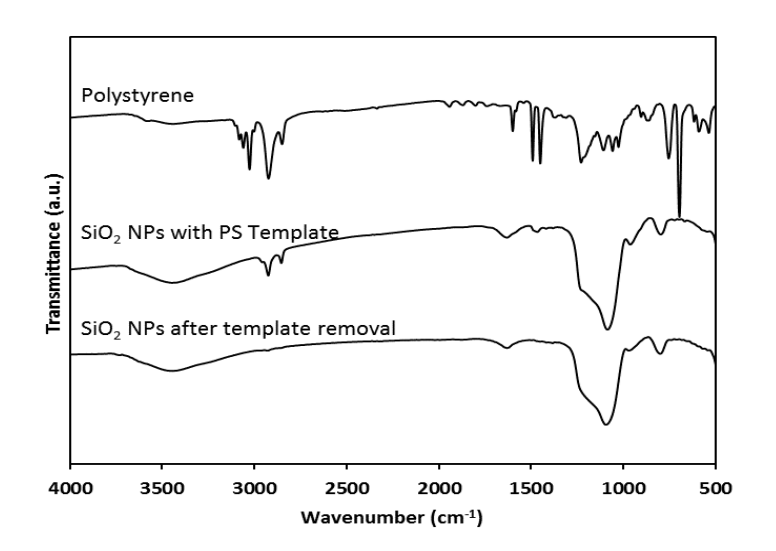


Figure 14. SEM micrographs of mesoporous silica nanoparticles synthesized at different amount of oil (a) 6 mL and (b) 8 mL

The polymer template was removed by calcination at 500 °C. Comparison of FT-IR spectrum of the mesoporous silica nanoparticles before and after template removal showed that the peaks that belonged to polystyrene disappeared after calcination. These results confirmed the removal of the polymer template as shown in **Figure 15**. In addition, TEM was used to characterize the mesoporous silica nanoparticles after calcination. **Figure 16** clearly showed pores inside the mesoporous silica nanoparticles.



**Figure 15.** FT-IR spectrum of mesoporous silica nanoparticles before and after template removal

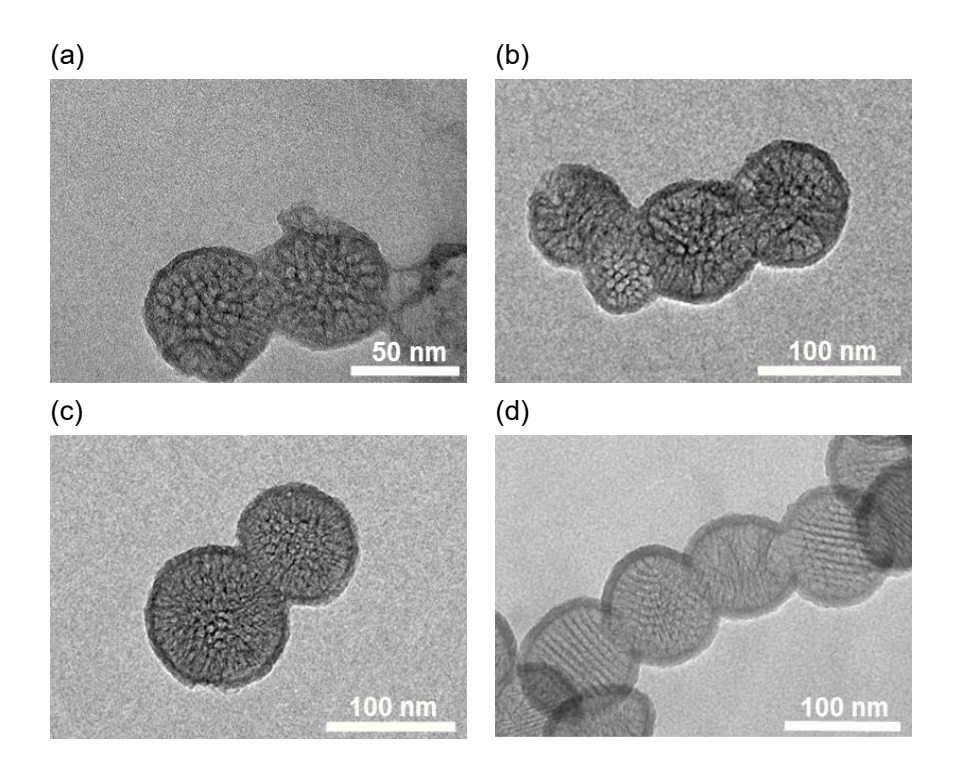
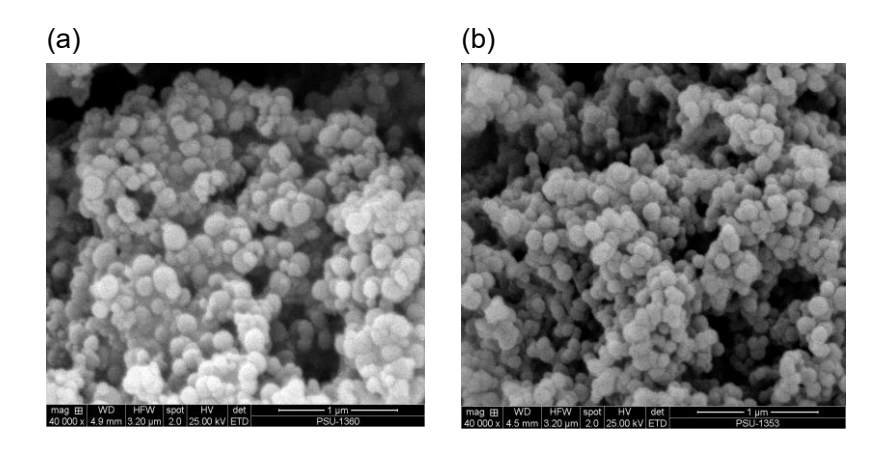


Figure 16. TEM images of mesoporous silica nanoparticles synthesized with different Styrene:TEOS volume ratios (a) 0.5:1, (b) 1:1, (c) 1.5:1, and (d) 2:1

Effect of methyl methacrylate concentration on the size of mesoporous silica nanoparticles was studied. By varying the amount of methyl methacrylate monomer, it can be seen that increasing the amount of methyl methacrylate monomer led to a decreasing of mesoporous silica nanoparticles, **Table 5** and the shape of the nanoparticles was distorted as shown in **Figure 17**.

**Table 5.** Synthesis condition of size of mesoporous silica nanoparticles using poly(methyl methacrylate) template at varied methyl methacrylate concentration

Sample	Water	Octane	MMA	TEOS	NH₄OH	Size
	(mL)	(mL)	(mL)	(mL)	(mL)	(nm)
Sample – 10	30	6	1.0	1.0	1.2	250±37
Sample – 11	30	8	2.0	1.0	1.2	197±26



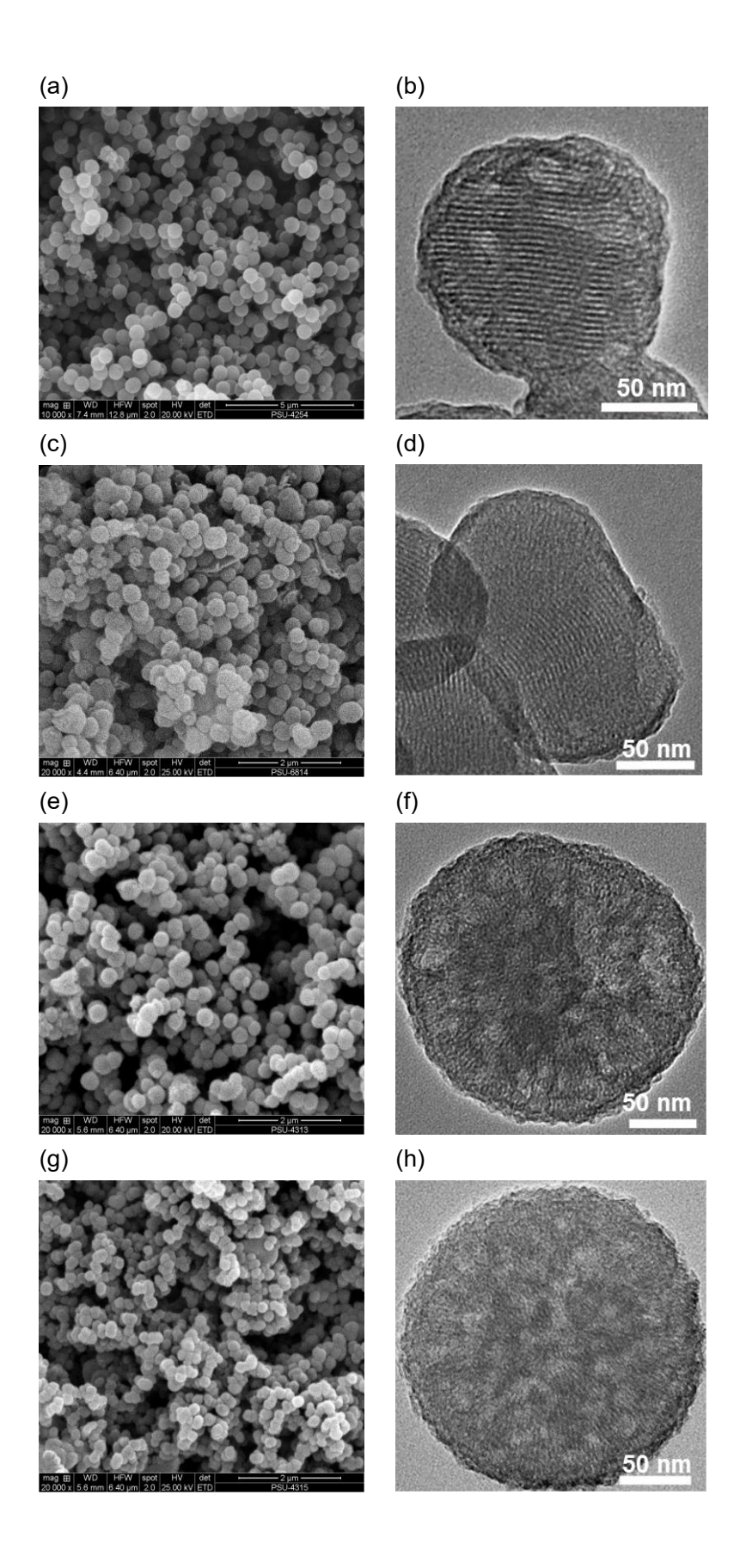
**Figure 17.** SEM micrographs of mesoporous silica nanoparticles synthesized with different MMA:TEOS volume ratios (a) 1:1 and (b) 2:1

### Surfactant Template

Effect of ethanol concentration on the size of mesoporous silica nanoparticles was studied. By varying the amount of ethanol concentration, it can be seen that decreasing the amount of ethanol concentration led to a decreasing of mesoporous silica nanoparticles, **Table 6** with a narrow size distribution. Moreover, the shape of the nanoparticles was spherical-like and the pore structure was lamellar at low ethanol concentration and changed to radial-like at higher ethanol concentration as shown in **Figure 18**.

**Table 6.** Synthesis condition of size of mesoporous silica nanoparticles using CTAB template at varied ethanol concentration

Sample	Water	EtOH	TEOS	NH₄OH	Size
	(mL)	(mL)	(mL)	(mL)	(nm)
Sample – 12	150	50	6.0	15.0	646±55
Sample – 13	160	40	6.0	15.0	303±51
Sample – 14	170	30	6.0	15.0	303±34
Sample – 15	180	20	6.0	15.0	201±23
Sample – 16	190	0	6.0	15.0	205±21



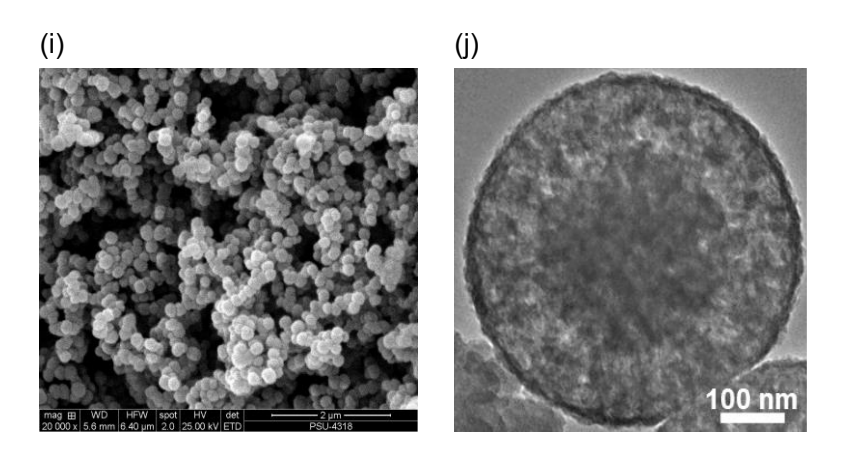


Figure 18. SEM and TEM micrographs of mesoporous silica nanoparticles synthesized with different H<sub>2</sub>O:EtOH volume ratios (a-b) 150:50, (c-d) 160:40, (e-f) 170:30, (g-h) 180:20, and (i-j) 190:0

#### Functionalization of mesoporous silica nanoparticles

## Polymer Template

Surface of mesoporous silica nanoparticles was functionalized with trimethyl (trifluoromethylsilane) to improve hydrophobicity of the nanoparticles. It can be seen that, the functionalization with short fluoroalkyl chain did not show significant effect on the size, **Table 7**. The shape of the mesoporous silica nanoparticles remained the same although short hair-like was observed around the surface of mesoporous silica nanoparticles under TEM, **Figure 19**.

**Table 7.** Synthesis condition of mesoporous silica nanoparticles functionalized with trimethyl(trifluoromethylsilane) (F3) at varied TEOS:F-Silane ratio

Sample	Water	Octane	TEOS	F-silane	NH₄OH	Size
	(mL)	(mL)	(mL)	(mL)	(mL)	(nm)
Sample – 17	30	8	1.0	0.13	1.2	115±19
Sample – 18	30	8	1.0	0.22	2.4	104±21
Sample – 19	30	8	1.0	0.67	3.6	122±17

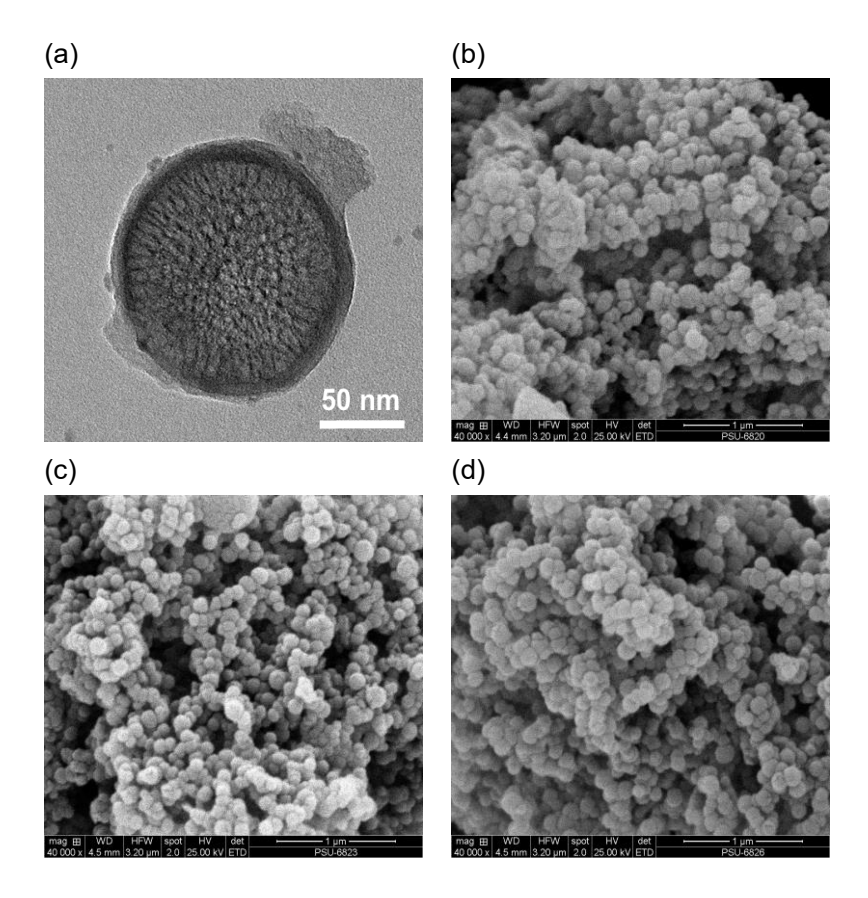
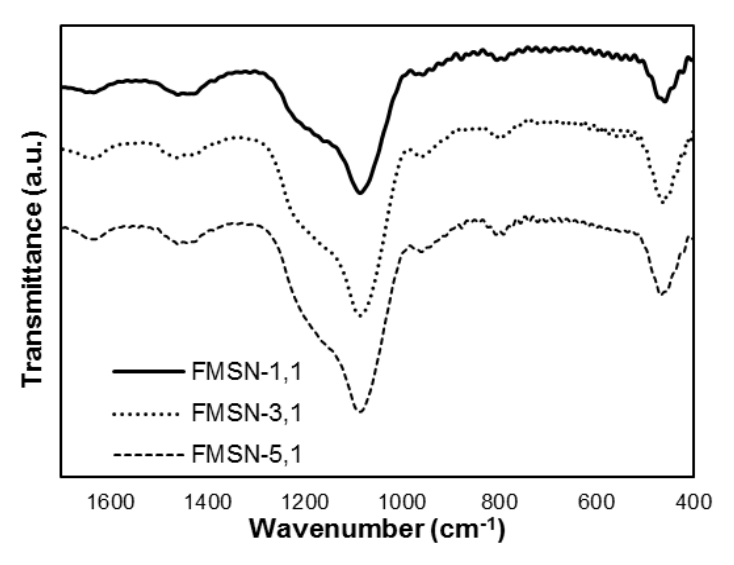
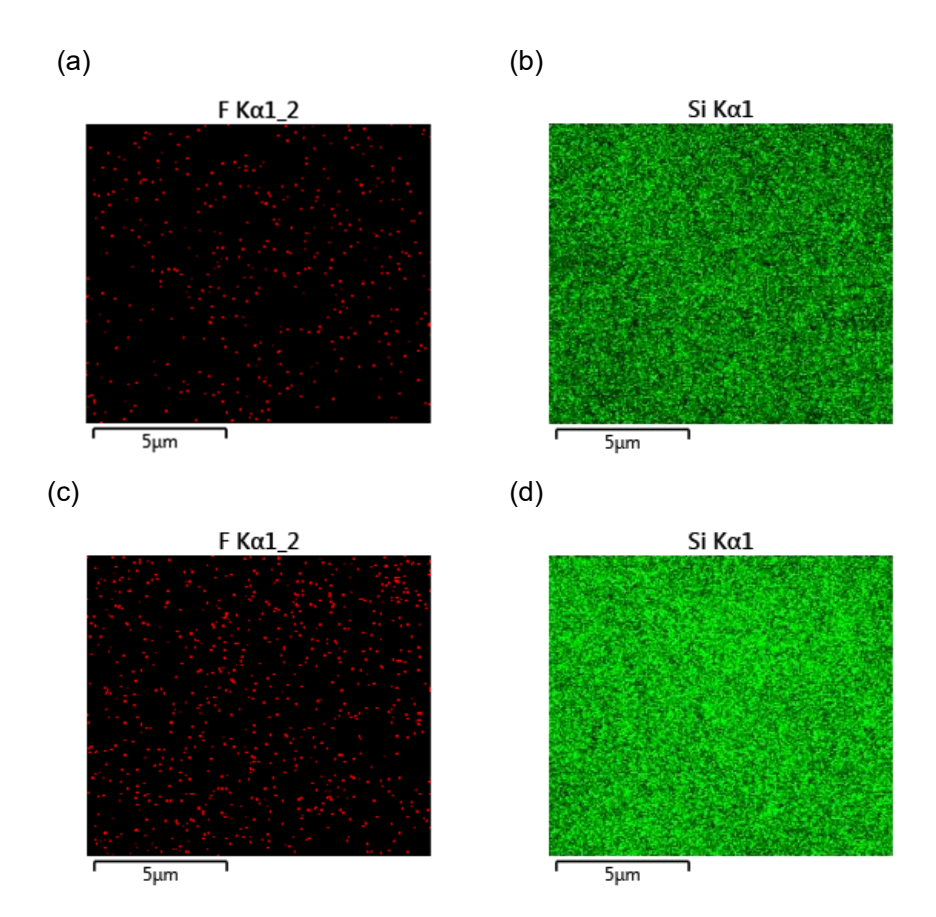


Figure 19. TEM and SEM micrographs of mesoporous silica nanoparticles functionalized with trimethyl(trifluoromethylsilane) (F3) at varied TEOS:F-Silane ratio (a-b) 5:1, (c) 3:1, and (d) 1:1

FT-IR was used to confirm surface functionalization with trimethyl(trifluoromethyl-silane), however, the peak shifting was not significant, **Figure 20**. Thus, SEM-EDX was used to characterize the surface functionalization which showed good dispersion of F-atom over the area of observation, **Figure 21**. In addition, an increasing of TEOS: F-Silane ratio led to significantly concentrate of F-atom in the SEM images.



**Figure 20.** FT-IR spectrum of mesoporous silica nanoparticles functionalized with trimethyl(trifluoromethylsilane) (F3) at varied TEOS:F-Silane ratio



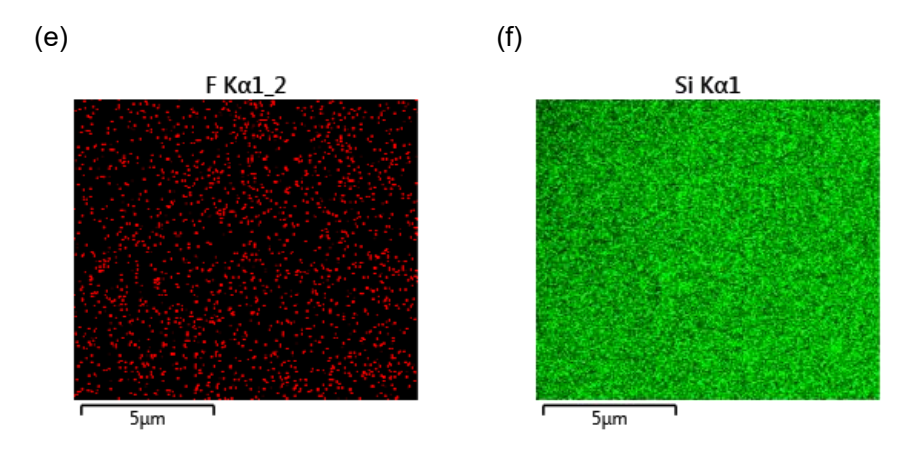


**Figure 21.** SEM-EDS spectroscopic mapping of mesoporous silica nanoparticles functionalized with trimethyl(trifluoromethylsilane) (F3) at varied TEOS:F-Silane ratio (a-b) 5:1, (c-d) 3:1, and (e-f) 1:1

Thermal stability of the MSNPs was characterized by simultaneous thermogravimetric analyzer (STA, PERKIN STA-8000) in air, from 25 - 900 °C with the heating rate of 10 °C/min. It can be seen that the mesoporous silica nanoparticles functionalized with trimethyl(trifluoromethylsilane) showed higher thermal stability compared to the mesoporous silica nanoparticles without surface functionalization, Figure 22. The surface area was calculated by using Brunauer-Emmett-Teller (BET) method and the pore size was obtained from Barrett-Joyner-Halenda (BJH) method. The mesoporous silica nanoparticles both before and after surface functionalization exhibited a typical type IV curves which was a characteristic of mesoporous materials. The results also suggested that surface functionalization by co-condensation with F-silane did not affect porous structure, Figure 23.

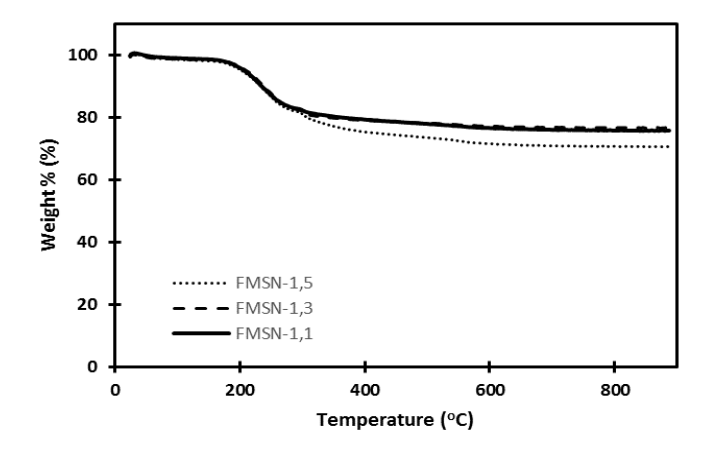


**Figure 22.** TGA thermograms of mesoporous silica nanoparticles functionalized with trimethyl(trifluoromethylsilane) (F3) at varied TEOS:F-Silane ratio

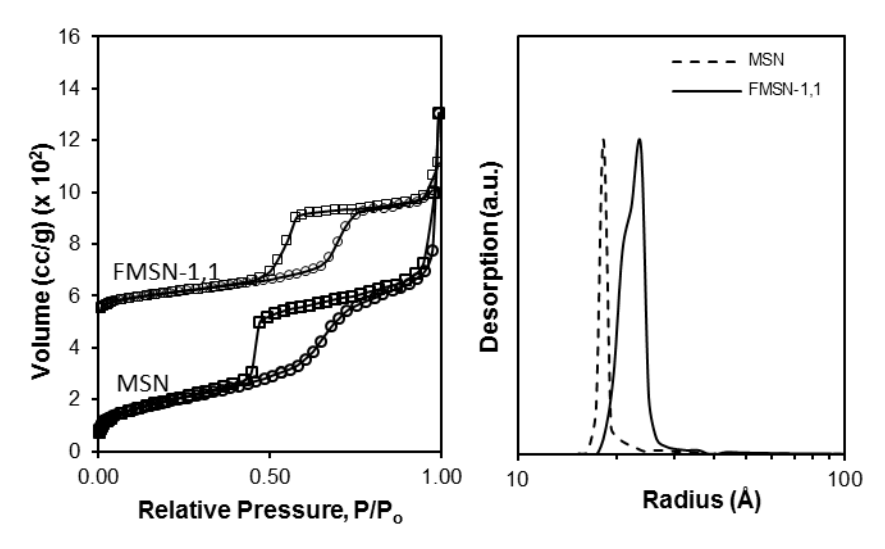


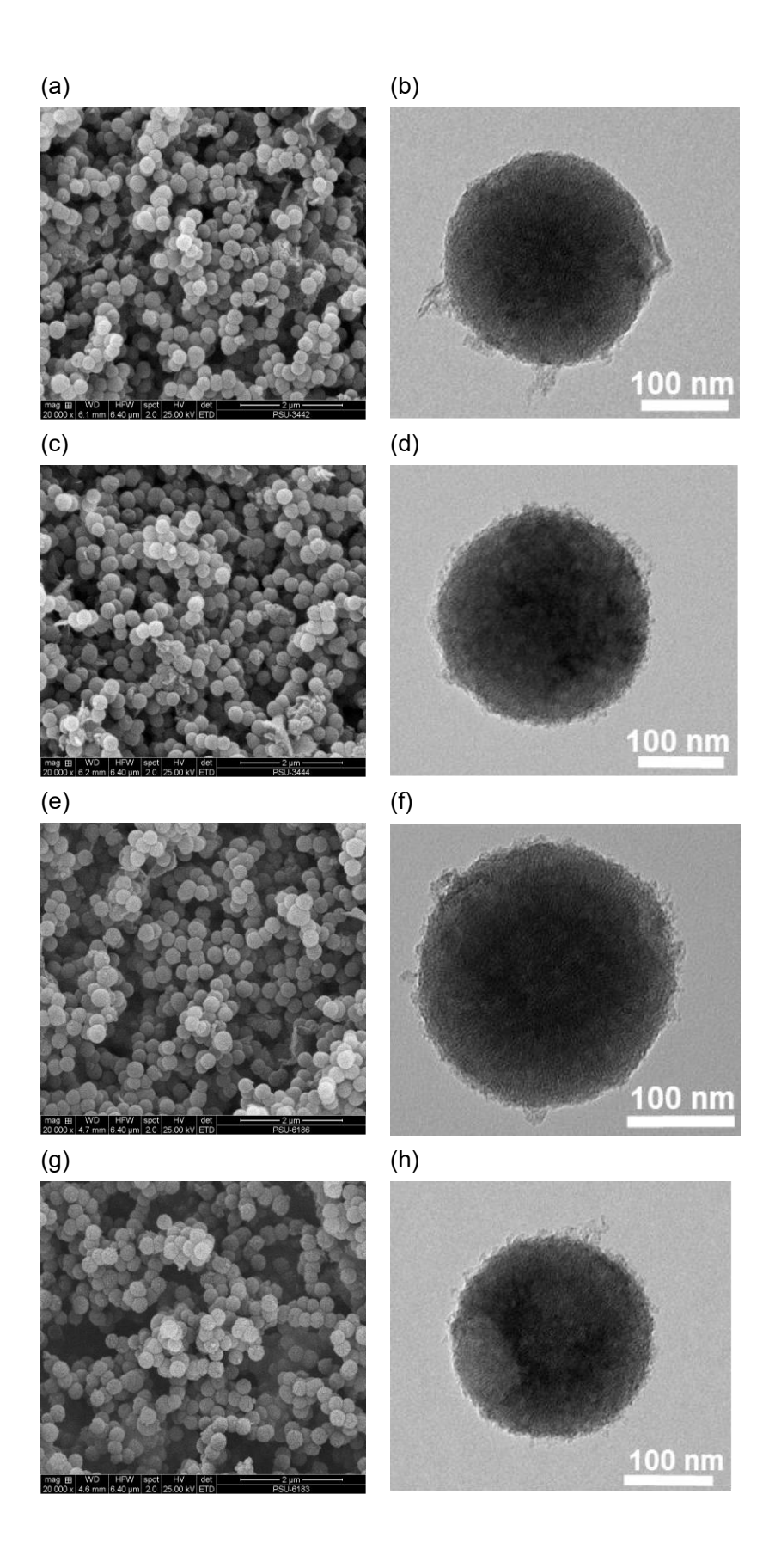
**Figure 23.** Nitrogen adsorption-desorption isotherms (a) (offset vertically by 500) and BJH pore size distribution curves (b) of mesoporous silica nanoparticles functionalized with trimethyl(trifluoromethylsilane) (F3)

#### Surfactant Template

Surface of mesoporous silica nanoparticles was functionalized with trimethyl (trifluoromethylsilane) and trichloro(1H,1H,2H,2H-perfluorooctyl)silane (F13) to improve hydrophobicity of the nanoparticles. It can be seen that, the functionalization with long fluoroalkyl chain rendered larger mesoporous silica nanoparticles, **Table 8**. The shape of the mesoporous silica nanoparticles remained the same and long hair-like was observed around the surface of mesoporous silica nanoparticles under TEM, **Figure 24**.

**Table 8.** Synthesis condition of mesoporous silica nanoparticles functionalized with trimethyl(trifluoromethylsilane) (F3) and trichloro(1H,1H,2H,2H-perfluorooctyl)silane (F13) at varied TEOS:F-Silane ratio

Sample	Water	EtOH	TEOS	F-silane	Size
	(mL)	(mL)	(mL)	(mL)	(nm)
Sample – 20	160	40	6.0	0.5, F3	287±22
Sample – 21	160	40	6.0	1.1, F3	291±18
Sample – 22	160	40	6.0	2.2, F3	298±27
Sample – 23	160	40	6.0	0.2, F13	290±22
Sample – 24	160	40	6.0	0.5, F13	317±24
Sample – 25	160	40	6.0	0.9, F13	368±56



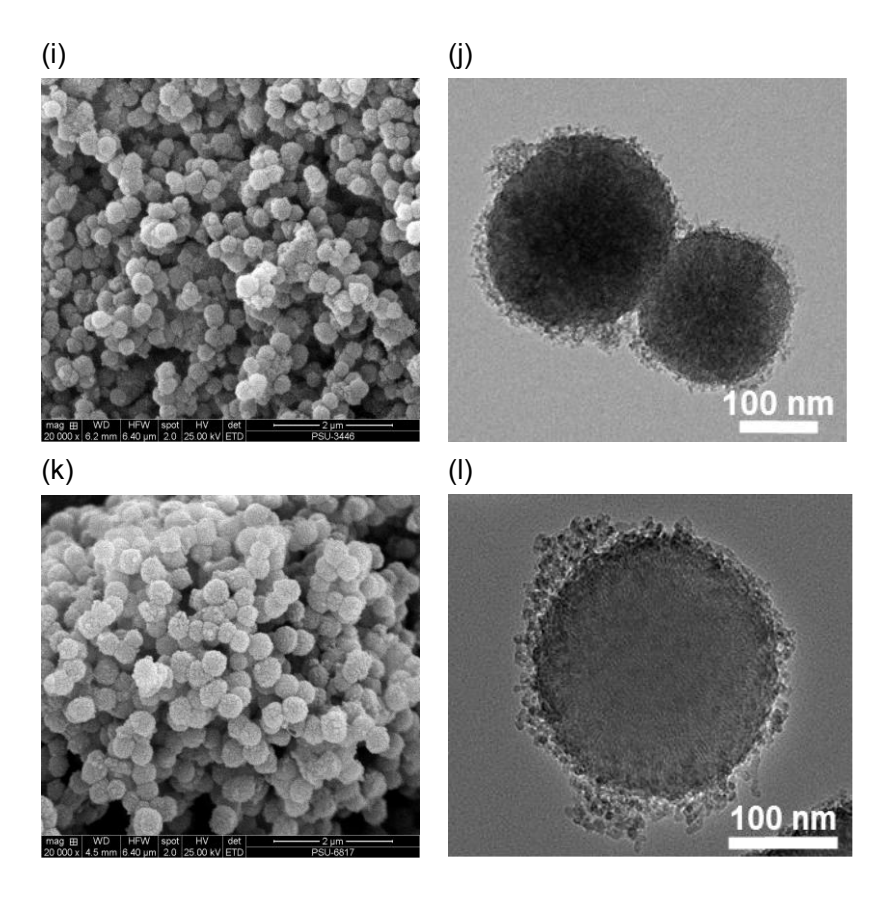
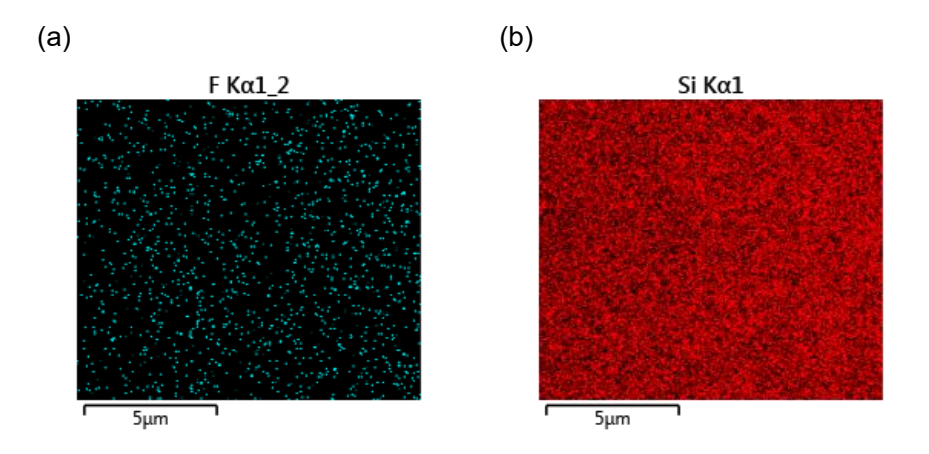
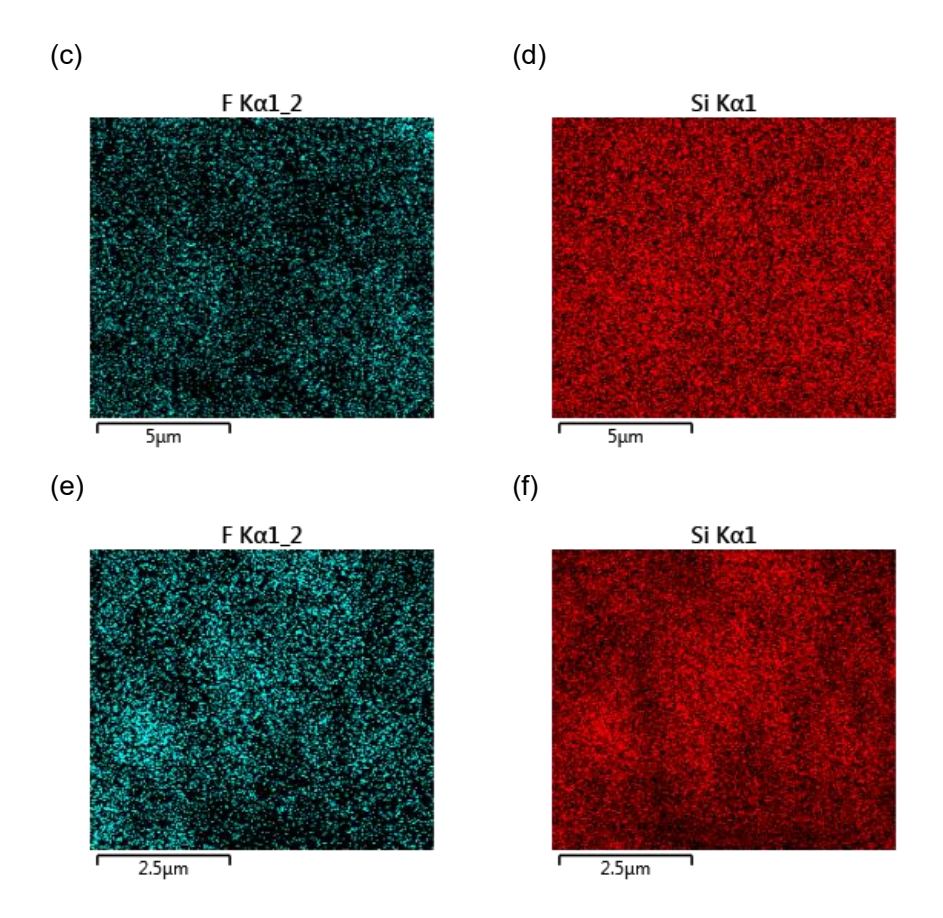


Figure 24. SEM and TEM micrographs of mesoporous silica functionalized with trimethyl(trifluoromethylsilane) (F3, a-f) and trichloro(1H,1H,2H,2H-perfluorooctyl)silane (F13, g-l) at varied TEOS:F-Silane ratio (a-b) F3-20:1, (c-d) F3-10:1, (e-f) F3-5:1, (g-h) F13-20:1, (i-j) F13-10:1, and (k-l) F13-5:1

SEM-EDX was used to characterize the surface functionalization, which showed good dispersion of F-atom over the area of observation, **Figure 25**. In addition, an increasing of TEOS:F-Silane ratio led to significantly concentrate of F-atom in the SEM images.





**Figure 25.** SEM-EDS spectroscopic mapping of mesoporous silica nanoparticles functionalized with trichloro(1H,1H,2H,2H-perfluorooctyl)silane (F13) at varied TEOS:F-Silane ratio (a-b) 20:1, (c-d) 10:1, and (e-f) 5:1

High resolution SEM images of the mesoporous silica nanoparticles functionalized with trimethyl(trifluoromethylsilane) and trichloro(1H,1H,2H,2H-perfluoro-octyl)silane are shown in **Figure 26**. Before surface functionalization, pores can be clearly observed on the surface, however, after surface functionalization with F-silane, the size of mesoporous silica nanoparticles increased significantly. In addition, the morphology of the particles changed from smooth surface to very rough surface due to the coating of long fluoroalkyl chain that generated nanostructure surface roughness.

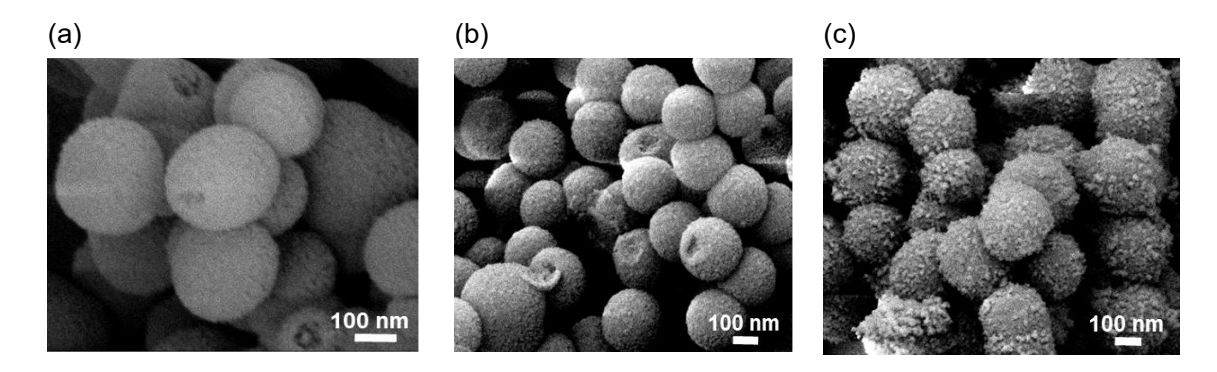


**Figure 26.** High resolution SEM micrographs of (a) bare mesoporous silica nanoparticles, (b) mesoporous silica nanoparticles functionalized with trimethyl(trifluoromethylsilane) (F3-5:1), and (c) mesoporous silica nanoparticles functionalized with trichloro(1H,1H,2H,2H-perfluorooctyl)silane (F13-5:1)

Thermal stabilities of the mesoporous silica nanoparticles with and without surface functionalization are shown in **Figure 27**. All samples display three major regions of weight-loss. The first region between 25 – 230 °C was attributed to the loss of moisture and the desorption of absorbed water in the pores of the mesoporous silica nanoparticles. The second region between 190 – 308 °C corresponded to the loss of residual CTAB inside the pores of the mesoporous silica nanoparticles and dihydroxylation of silanol. The third region between 300 – 511 °C corresponded to the loss of residual remaining organic fragments and decomposition of fluoroalkyl fragments. Moreover, it can be seen that the mesoporous silica nanoparticles functionalized with trichloro(1H,1H,2H,2H-perfluorooctyl)silane showed higher thermal stability compared to the mesoporous silica nanoparticles without surface functionalization.

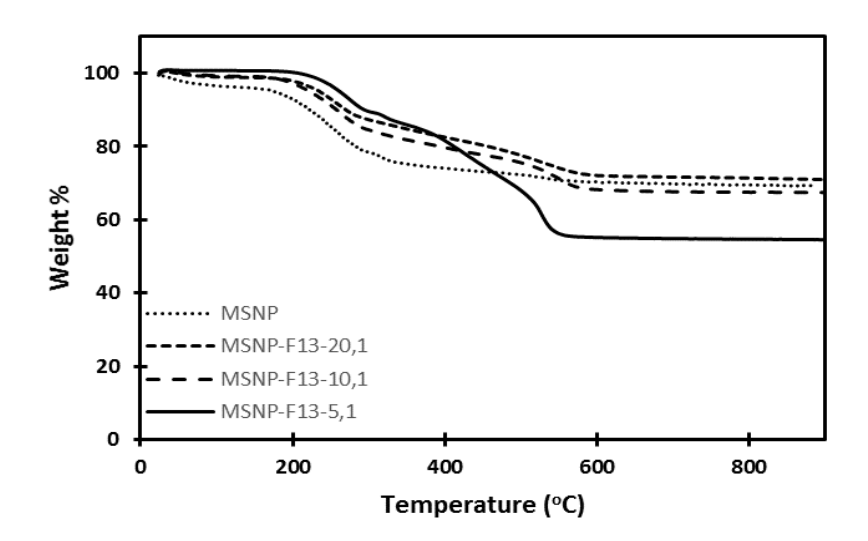


**Figure 27.** TGA thermograms of mesoporous silica nanoparticles functionalized with trichloro(1H,1H,2H,2H-perfluorooctyl)silane (F13) at varied TEOS:F-Silane ratio

Figure 28 shows adsorption/desorption isotherms of the mesoporous silica nanoparticles with lamellar pore structure and radial-like pore structure before and after surface functionalization with trichloro(1H,1H,2H,2H-perfluorooctyl)silane. It can be seen that all samples exhibited a typical type IV curves, which was a characteristic of mesoporous materials. The pore radius of the mesoporous silica nanoparticles was about 54 Å for lamellar-pore MSNPs and in the range of 20-22 Å for radial-pore MSNPs indicating very narrow mesoporous nanoparticles.

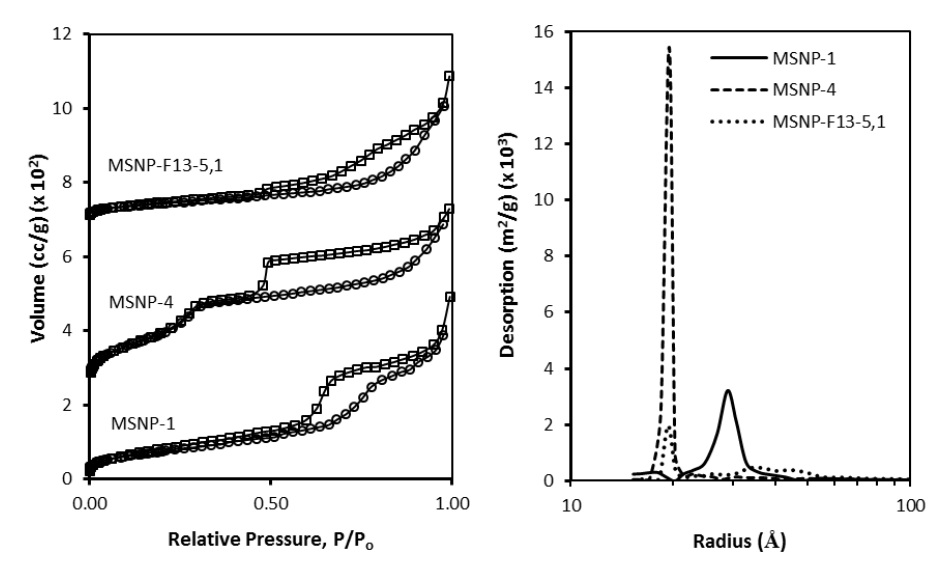


**Figure 28.** Nitrogen adsorption-desorption isotherms (a) (offset vertically by 200 and 700 for MSNP-4 and MSNP-F<sub>13</sub>-5,1, respectively) and BJH pore size distribution curves (b) of MSNPs

#### Surface coating with mesoporous nanoparticles

#### Polymer Template

AFM images of glass substrate coated with mesoporous silica nanoparticles are shown in **Figure 29**. It can be seen that the coated substrate with fluoroalkyl functionalized mesoporous silica nanoparticles had rough surface with the RMS of 0.167 nm.

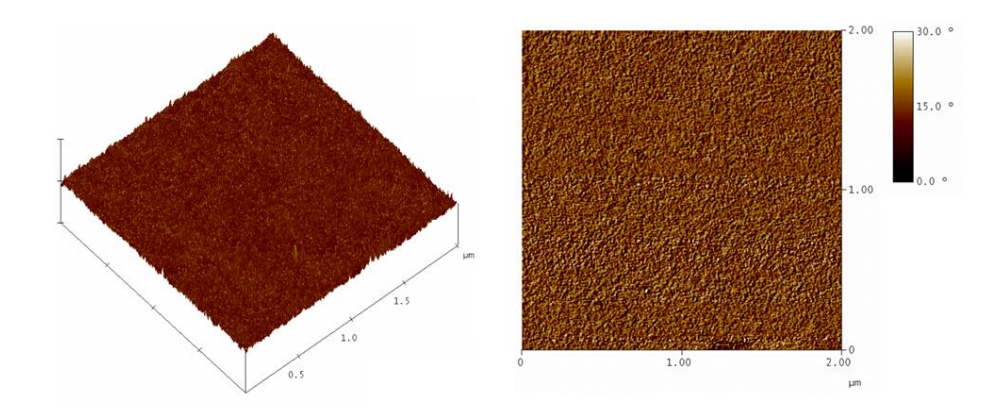


**Figure 29.** AFM images of glass substrates coated with mesoporous silica nanoparticles functionalized with trimethyl(trifluoromethylsilane) (F3) at TEOS:F-Silane ratio 5:1

Water contact angles (CAs) of a glass substrate coated with mesoporous silica nanoparticles and photographs of a water droplet on the substrate were shown in **Table 19** and **Figure 30**, respectively. It is obvious that the coated substrate with fluoroalkyl functionalized mesoporous silica nanoparticles improved hydrophobicity of the substrate in such a way that the water CAs, both advancing CA and receding CA, increased significantly.

**Table 9.** Water contact angles of glass substrates coated with mesoporous silica nanoparticles functionalized with trimethyl(trifluoromethylsilane) (F3) at varied TEOS: F-Silane ratio

Sample	TEOS:F-silane	Advancing (°)	Receding (°)
Sample – 5	1:0	64.3	23.9
Sample – 17	20:1	99.4	23.0
Sample – 18	10:1	126.6	48.8
Sample – 19	5:1	113.8	41.5

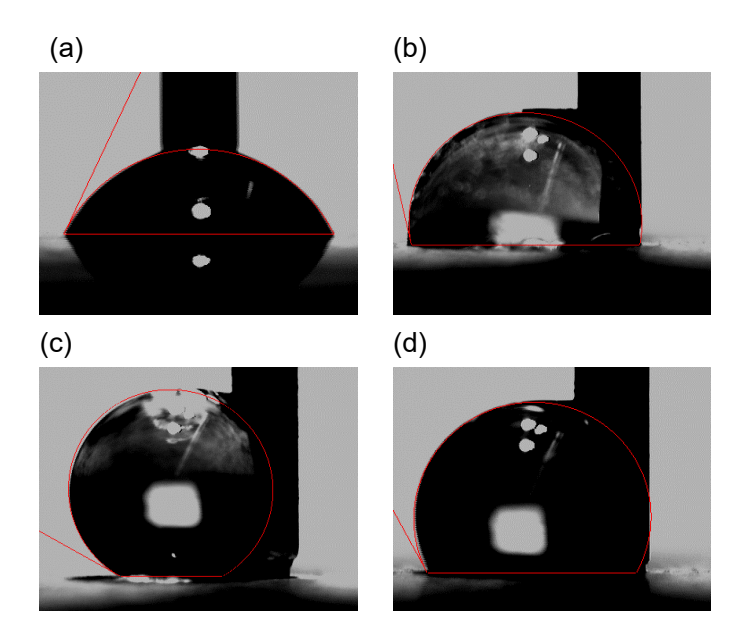


Figure 30. Photographs of water droplets on glass substrates coated with mesoporous silica nanoparticles functionalized with trimethyl(trifluoromethylsilane) (F3) at varied TEOS:F-Silane ratio (a) 1:0, (b) 5:1, (c) 3:1, and (d) 1:1

#### Surfactant Template

Water contact angles (CAs) of a glass substrate coated with mesoporous silica nanoparticles and photographs of a water droplet on the substrate were shown in **Table 10** and **Figure 31**, respectively. It is obvious that the coated substrate with fluoroalkyl functionalized mesoporous silica nanoparticles improved hydrophobicity of the substrate in such a way that the water CAs, both advancing CA and receding CA, increased significantly. Increasing mole ratio of F-silane tends to increase CAs of the substrates. Moreover, the mesoporous silica nanoparticles functionalized with long fluoroalkyl chain, trichloro(1H,1H,2H,2H-perfluorooctyl)silane (F13), resulted in much higher CAs compared to those of shorter fluoroalkyl chain, trimethyl(trifluoromethylsilane) (F3). Sample – 25 imparted average advancing CA of 152.7° with the highest value of 158.6° which is a characteristic of super-hydrophobic and oleophobic material. These results were consistent with the morphology of the MSNPs as shown in TEM images that the fluoroalkyl shell was thicker when the surface of the MSNPs was functionalized with trichloro(1H,1H,2H,2H-perfluorooctyl)silane (F13).

**Table 10.** Water contact angles of glass substrates coated with mesoporous silica nanoparticles functionalized with trimethyl(trifluoromethylsilane) (F3) and trichloro-(1H,1H,2H,2H-perfluorooctyl)silane (F13) at varied TEOS:F-Silane ratio

Sample	TEOS:F-silane	Advancing (°)	Receding (°)
Sample – 13	1:0	46.3	24.1
Sample – 20	20:1, F3	60.8	20.9
Sample – 21	10:1, F3	66.3	26.5
Sample – 22	5:1, F3	68.9	23.8
Sample – 23	20:1, F13	92.4	40.8
Sample – 24	10:1, F13	126.5	33.7
Sample – 25	5:1, F13	152.7	73.7

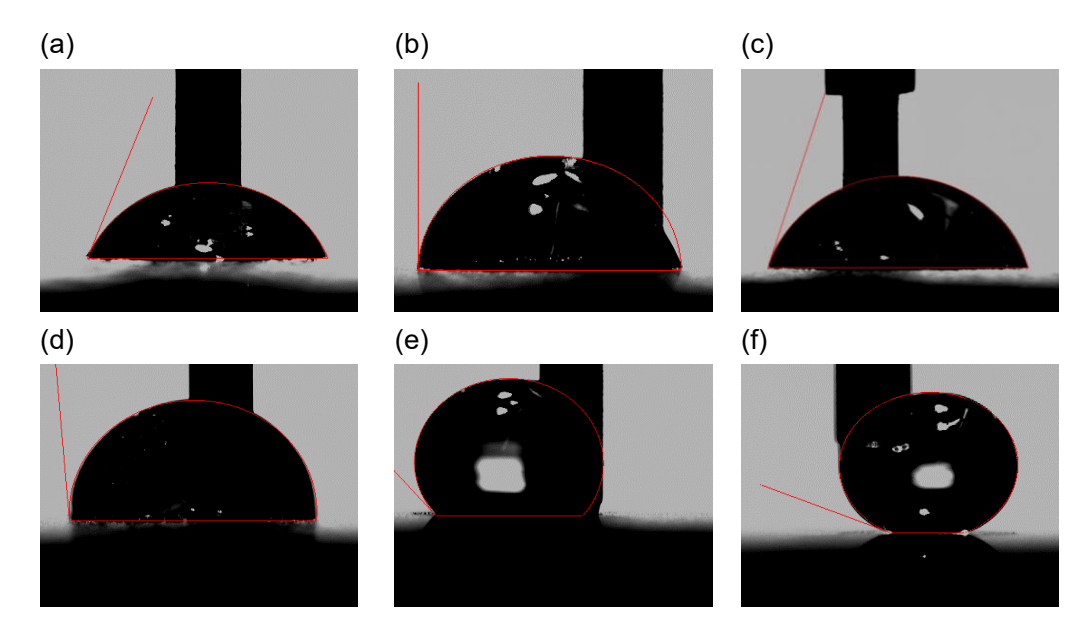


**Figure 31.** Photographs of water droplets on glass substrates coated with mesoporous silica nanoparticles functionalized with trimethyl(trifluoromethylsilane) (F3, a-c) and trichloro(1H,1H,2H,2H-perfluorooctyl)silane (F13, d-f) at varied TEOS:F-Silane ratio (a,d) 20:1, (b,e) 10:1, and (c,f) 5:1

### Conclusion

The spherical with mesoporous silica nanoparticles with narrow size distribution were synthesized successfully using polymer and surfactant templates. Increasing volume ratio of EtOH and polymer concentration resulted in both an enlargement of the particles and changing pore structure inside the particles from a lamellar structure to a

radially oriented structure. Surface wettability of the mesoporous silica nanoparticles was improved by functionalization with two different types of fluoroalkyl silane. The mesoporous silica nanoparticles formed a core-shell structure after co-condensation with F-silane. Increasing mole ratio of F-silane generated thick and dense hair-like shell, thus, the morphology of the particles changed from smooth surface to very rough surface. Water CA measurement proved that hydrophobicity and oleophobicity of the particles were improved after the chemical modification with F13-silane. Therefore, they show potentiality to be used in coating applications.

### References

- (1) Huang, C.; Taipei, N. Method of Manufacturing an Anti-Fingerprint Paint and Use of the Anti-Fingerprint Paint, **2012**.
- (2) Navarrini, W.; Brivio, T.; Capobianco, D.; Diamanti, M. V.; Pedeferri, M.; Magagnin, L.; Resnati, G. Anti-Fingerprints Fluorinated Coating for Anodized Titanium Avoiding Color Alteration. J. Coatings Technol. Res. 2010, 8, 153–160.
- Wu, L. Y. L.; Ngian, S. K.; Chen, Z.; Xuan, D. T. T. Quantitative Test Method for Evaluation of Anti-Fingerprint Property of Coated Surfaces. *Appl. Surf. Sci.* 2011, 257, 2965–2969.
- (4) Fiore, D.; Wilson, B. Hydrophobic and Oleophobic Coating Technologies for Polymer Optics. *Polym. Opt. Molded Glas. Opt.* **2012**, *8489*, 84890G–84890G–7.
- Yildirim, A.; Budunoglu, H.; Daglar, B.; Deniz, H.; Bayindir, M. One-Pot Preparation of Fluorinated Mesoporous Silica Nanoparticles for Liquid Marble Formation and Superhydrophobic Surfaces. ACS Appl. Mater. Interfaces 2011, 3, 1804–1808.
- (6) Yabu, H.; Shimomura, M. Single-Step Fabrication of Transparent Superhydrophobic Porous Polymer Films. *Chemistry* **2005**, *17*, 5231–5234.
- (7) Tuteja, A.; Choi, W.; Ma, M.; Mabry, J. M.; Mazzella, S. a; Rutledge, G. C.; McKinley, G. H.; Cohen, R. E. Designing Superoleophobic Surfaces. *Science*. 2013, 318, 1618–1622.
- (8) Cao, L.; Gao, D. Transparent Superhydrophobic and Highly Oleophobic Coatings. *Faraday Discuss.* **2010**, *146*, 57–65.
- (9) Nishino, T.; Meguro, M.; Nakamae, K. Poly(Vinyl Alcohol) with Low Surface Free Energy by Fluorination. *Adhes. Adhes.* 1999, 19, 399–403.

- (10) Hsieh, C.-T.; Chen, W.-Y.; Wu, F.-L.; Shen, Y.-S. Fabrication and Superhydrophobic Behavior of Fluorinated Silica Nanosphere Arrays. *J. Adhes. Sci. Technol.* **2008**, 22, 265–275.
- (11) Ramos, S. M. M.; Benyagoub, A.; Canut, B.; Jamois, C. Superoleophobic Behavior Induced by Nanofeatures on Oleophilic Surfaces. *Langmuir* **2010**, *26*, 5141–5146.
- (12) Coulson, S. R.; Woodward, I.; Badyal, J. P. S.; Brewer, S. A.; Willis, C.; Down, P.; Ojq, S. S. P. Super-Repellent Composite Fluoropolymer Surfaces. *J. Phys. Chem. B* 2000, 104, 8836–8840.
- (13) Wenzel, R. N. Resistance of Solid Surfaces to Wetting by Water. *Ind. Eng. Chem.* **1936**, 28, 988–994.
- (14) Cassie, B. D.; Baxter, S. Wettability of Porous Surfaces. *Trans. Faraday Soc.* **1944**, 40, 546–551.
- (15) Shang, H. M.; Wang, Y.; Limmer, S. J.; Chou, T. P.; Takahashi, K.; Cao, G. Z. Optically Transparent Superhydrophobic Silica-Based Films. *Thin Solid Films* **2005**, 472, 37–43.
- (16) Cao, L.; Hu, H.-H.; Gao, D. Design and Fabrication of Micro-Textures for Inducing a Superhydrophobic Behavior on Hydrophilic Materials. *Langmuir* 2007, 23, 4310– 4314.
- (17) Tadanaga, K.; Katata, N.; Minami, T. Formation Process of Super-Water-Repellent Al 2 O 3 Coating Films with High Transparency by the Sol – Gel Method. J. Am. Ceram. Soc. 1997, 80, 3213–3216.
- (18) Tadanaga, K.; Katata, N.; Minami, T. Super-Water-Repellent Al<sub>2</sub>O<sub>3</sub> Coating Films with High Transparency. *J. Am. Ceram. Soc.* **1997**, *80*, 1040–1042.
- (19) Erbil, H. Y.; Demirel, a L.; Avci, Y.; Mert, O. Transformation of a Simple Plastic into a Superhydrophobic Surface. *Science* **2003**, *299*, 1377–1380.
- (20) Onda, T.; Shibuichi, S.; Satoh, N.; Tsujii, K. Super-Water-Repellent Fractal Surfaces. *Langmuir* **1996**, *12*, 2125–2127.
- (21) Nakajima, A.; Abe, K.; Hashimoto, K.; Watanabe, T. Preparation of Hard Super-Hydrophobic Films with Visible Light Transmission. *Thin Solid Films* **2000**, *376*, 140–143.

- (22) Teshima, K.; Sugimura, H.; Inoue, Y.; Takai, O.; Takano, A. Transparent Ultra Water-Repellent Poly(ethylene Terephthalate) Substrates Fabricated by Oxygen Plasma Treatment and Subsequent Hydrophobic Coating. *Appl. Surf. Sci.* **2005**, *244*, 619–622.
- (23) Ohkubo, Y.; Tsuji, I.; Onishi, S.; Ogawa, K. Preparation and Characterization of Super-Hydrophobic and Oleophobic Surface. *J. Mater. Sci.* **2010**, *45*, 4963–4969.
- (24) Brassard, J.-D.; Sarkar, D. K.; Perron, J. Synthesis of Monodisperse Fluorinated Silica Nanoparticles and Their Superhydrophobic Thin Films. *ACS Appl. Mater. Interfaces* **2011**, *3*, 3583–3588.
- (25) Bravo, J.; Zhai, L.; Wu, Z.; Cohen, R. E.; Rubner, M. F. Transparent Superhydrophobic Films Based on Silica Nanoparticles. *Langmuir* **2007**, *23*, 7293–7298.
- (26) Su, C.; Li, J.; Geng, H.; Wang, Q.; Chen, Q. Fabrication of an Optically Transparent Super-Hydrophobic Surface via Embedding Nano-Silica. *Appl. Surf. Sci.* **2006**, *253*, 2633–2636.
- (27) Lu, Y.; Fan, H.; Stump, A.; Ward, T. L.; Rieker, T.; Brinker, C. J. Aerosol-Assisted Self- Assembly of Mesostructured Spherical Nanoparticles. *Nature* **1999**, *398*, 223–226.
- (28) Kim, S. H.; Liu, B. Y. H.; Zachariah, M. R. Ultrahigh Surface Area Nanoporous Silica Particles via an Aero-Sol-Gel Process. *Langmuir* **2004**, *20*, 2523–2526.
- (29) Iskandar, F.; Okuyama, K. Controllability of Pore Size and Porosity on Self-Organized Porous Silica Particles. *Nano Lett.* **2002**, *2*, 389–392.
- (30) MAO Zheng-wei, H. L. Z. Q. G. C. Fabrication of Porous Silica Microspheres Under the Assistance of Solid Template. *Chem. Res. CHINESE Univ.* **2012**, 28, 546–549.
- (31) Brassard, J.-D.; Sarkar, D. K.; Perron, J. Fluorine Based Superhydrophobic Coatings. *Appl. Sci.* **2012**, 2, 453–464.
- (32) Nakajima, A.; Hashimoto, K.; Watanabe, T. Transparent Superhydrophobic Thin Films with Self-Cleaning Properties. *Langmuir* **2000**, *16*, 7044–7047.

# **APPENDIX**

### Output จากโครงการวิจัยที่ได้รับทุนจาก สกว.

- การเสนอผลงานแบบโปสเตอร์ งานประชุมวิชาการ The International Polymer Conference of Thailand: PCT-6 ณ โรงแรมปทุมวันปริ้นเซส กรุงเทพฯ เมื่อวันที่ 30 มิถุนายน – 1 กรกฎาคม 2559
- 2. ผลงานตีพิมพ์ในวารสารวิชาการนานาชาติ

Sirinya Chantarak, Jooyoung Chang, Sumetha Suwanboon, Saad Riyajan Journal of Porous Materials, 2017

DOI: https://doi.org/10.1007/s10934-017-0551-6

First Online: 26 December 2017

### หนังสือตอบรับเพื่อนำเสนอผลงานแบบโปสเตอร์ งานประชุมวิชาการ The International Polymer Conference of Thailand: PCT-6 ณ โรงแรมปทุมวันปริ้นเซส กรุงเทพฯ เมื่อวันที่ 30 มิถุนายน – 1 กรกฎาคม 2559



-[PCT-6]-

http://www.thaipolymersociety.org/pct-6/index.html

Polymer Society of Thailand NSTDA Building, Ministry of Science and Technology, Rama 6 Road, Bangkok 10400, Thailand

June 9, 2016

Dear Sirinya Chantarak,

The 6<sup>th</sup> International Polymer Conference of Thailand (PCT-6) is pleased to inform you that your paper entitled "An Economical Route to Synthesize Mesoporous Silica Nanoparticles" has been accepted for poster presentation at the PCT-6 conference. This decision is made based on a peer review process. The conference will be held in Pathumwan Princess Hotel, Bangkok, Thailand, between June 30 – July 1, 2016.

Authors of accepted papers are invited to register, make payment, attend and present their research paper at one of the conference sessions. Presented papers are eligible for publication in the conference proceedings.

We are looking forward to welcoming you soon.

Yours sincerely,

Prof. Suwabun Chirachanchai, Ph.D.

Professor

Conference Chair & President of Polymer Society of Thailand

บทคัดย่อการนำเสนอผลงานแบบโปสเตอร์

งานประชุมวิชาการ The International Polymer Conference of Thailand: PCT-6

ณ โรงแรมปทุมวันปริ้นเซส กรุงเทพฯ เมื่อวันที่ 30 มิถุนายน – 1 กรกฎาคม 2559

An Economical Route to Synthesize Mesoporous Silica Nanoparticles

Sirinya Chantarak<sup>1\*</sup>, Sumetha Suwanboon<sup>1</sup>, Saad Riyajan<sup>2</sup>

<sup>1</sup>Department of Materials Science and Technology, Faculty of Science,

Prince of Songkla University, Songkhla 90112

<sup>2</sup>Department of Chemistry, Faculty of Science and Technology, Thammasat University,

Pathumthani 12120

Phone +6674288364, Fax +6674446925, \*E-mail: sirinya.c@psu.ac.th

**Abstract** 

Several methods have been used to prepare mesoporous particles for varieties

of application including catalytic supports, sorbents, sensors, and surface modifiers. This

research provided an alternating pathway to synthesize mesoporous silica nanoparticles

(MSNPs) via emulsion polymerization. MSNPs in the range of 100 - 300 nm were

synthesized using simultaneously-generated polystyrene template. Scanning electron

micrographs revealed spherical nanoparticles with narrow size distribution. The template

was extracted by a cost-effective post-chemical treatment using selective solvents

without a requirement of sophisticated equipment yielding MSNPs. Fourier-Transform

Infrared Spectroscopy and Transmission Electron Microscopy were employed to confirm

the removal of the template and the formation of lamella and hexagonal mesopores

within the particles. In this work, effect of initiator concentration, reaction time, and

template-monomer concentration on size and structural morphology of MSNPs were

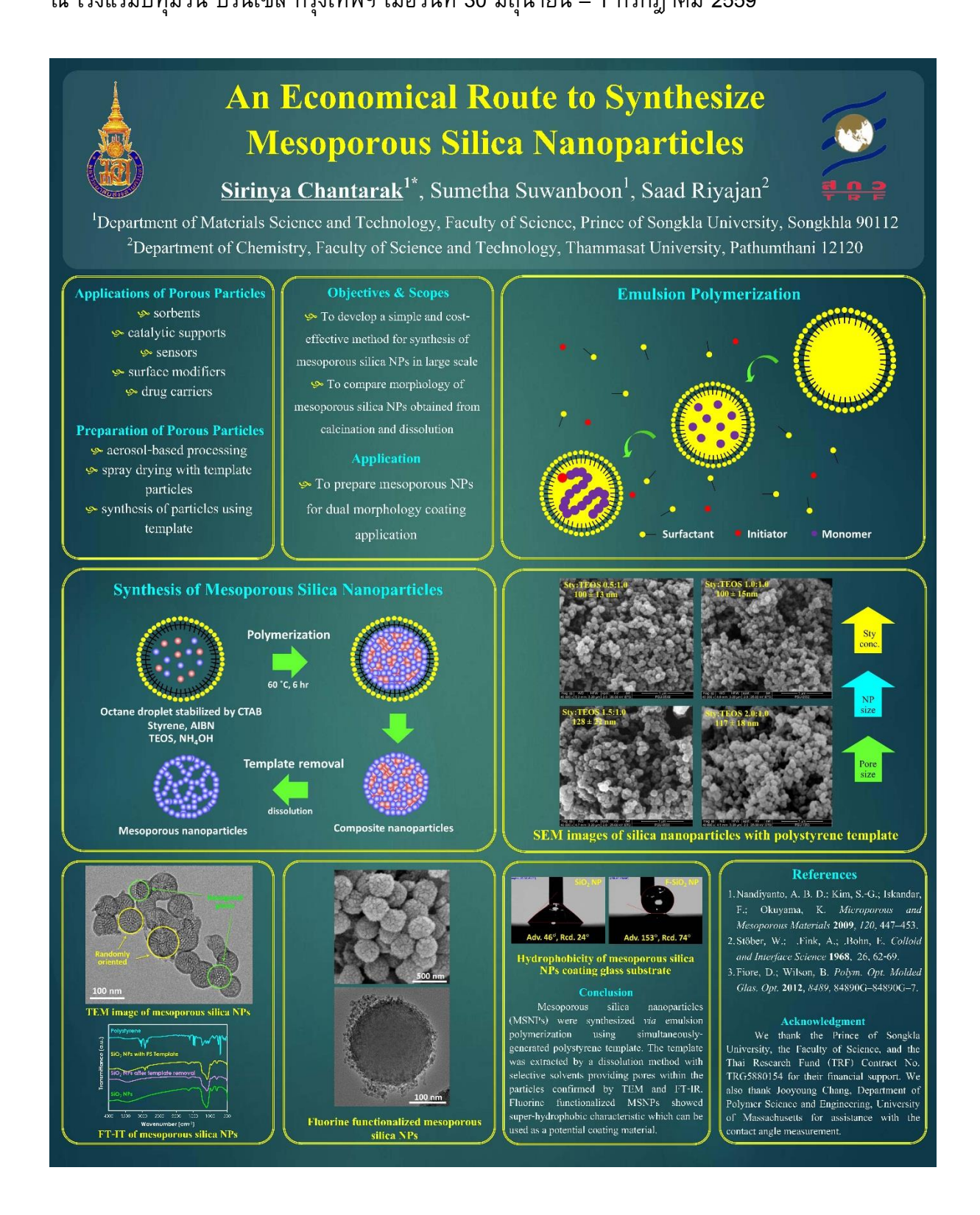
investigated. This research can be applied as a potential model for synthesis of

controlled size and pore size of the porous nanoparticles.

**Keywords:** Silica Porous Nanoparticle Emulsion Polystyrene

37

### โปสเตอร์การนำเสนอผลงานแบบโปสเตอร์ งานประชุมวิชาการ The International Polymer Conference of Thailand: PCT-6 ณ โรงแรมปทุมวัน ปริ้นเซส กรุงเทพฯ เมื่อวันที่ 30 มิถุนายน – 1 กรกฎาคม 2559





## Synthesis of superhydrophobic core-shell mesoporous silica nanoparticles

Sirinya Chantarak<sup>1</sup> • Jooyoung Chang<sup>2</sup> · Sumetha Suwanboon<sup>1</sup> · Saad Riyajan<sup>3</sup>

© Springer Science+Business Media, LLC, part of Springer Nature 2017

#### **Abstract**

Mesoporous silica nanoparticles (MSNPs) have been used in variety of applications due to their morphology and porous structure. This work reports the one-pot synthesis of ultrahydrophobic MSNPs using *N*-cetyl-*n*,*n*,*n* trimethyl ammonium bromide as a cationic surfactant template and ethanol (EtOH) as a cosolvent to form mesopores in the MSNPs. The effects of EtOH on the size and the pore structure of the MSNPs were studied by scanning electron microscopy and transmission electron microscopy. The results show that an addition of EtOH led to an enlargement of the MSNPs and a change in pore structure from a lamellar structure to a radially oriented structure. Co-condensation with two different types of fluoroalkyl silanes; trimethyl(fluoromethyl)silane, and trichloro(*1H*,*1H*,*2H*,*2H*-perfluorooctyl)silane provided low surface energy MSNPs with a core–shell structure. An assembly on the surface of these F-MSNPs generated nanostructure surface roughness rendering an improvement in surface wettability with water contact angle of 158.6°, which is a characteristic of oleophobic and ultrahydrophobic material.

**Keywords** Silica nanoparticle · Core–shell · Porous material · Hydrophobic · Self-assembly

### 1 Introduction

Silica is an attractive material providing interesting characteristics including high thermal stability, chemical inert, low toxicity, and biocompatibility [1, 2]. The synthesis of the mesoporous silica was first reported in 1992 by Kresge et al. [3, 4]. The methods to provide the monodispersed mesoporous silica nanoparticles (MSNPs) have been developing by many research groups such as the use of solid template [5], soft template [6–11], microwave synthesis [12], and an aerosol process [13]. Various strategies of synthesis method and types of template lead to different morphologies of the mesoporous silica such as thin film, fiber, and sphere

[14] and a wide array of pore structures such as hexagonal pore structure, cubic pore structure, and lamellar pore structure.

Surfactant templating is an alternating technique to synthesize the MSNPs [4, 15] in which pore size and diameter of particles can be adjusted by changing the type and the concentration of silica source and surfactant [16–18]. Furthermore, the addition of a cosolvent [16, 18, 19], the adjustment of solution temperature [6], and the pH of a solution using different base [16–18, 20] were also reported to exhibit significant effects on the pore size and the morphology of the MSNPs as well.

To date, the ordered MSNPs have been utilized in various applications due to their morphology and uniformity of pore structure. The MSNPs impart high specific surface area, which is desired for potential applications including catalyst supporter [21], cell imaging [22], drug carrier [23, 24], absorbent, and chromatography [25]. Controlling shape and size of particles, pores, and their structure are pivotal especially for specific uses such as size-selective filters [26, 27], and controlled drug release [28, 29]. The MSNPs have been also used in a coating application. The synthesis of hydrophobic MSNPs has been reported by many research groups. Those MSNPs were prepared by using co-condensation or

Published online: 26 December 2017



<sup>⊠</sup> Sirinya Chantarak sirinya.c@psu.ac.th

Department of Materials Science and Technology, Faculty of Science, Prince of Songkla University, Songkhla 90110, Thailand

Department of Polymer Science and Engineering, University of Massachusetts, Amherst, MA 01003, USA

Department of Chemistry, Faculty of Science and Technology, Thammasat University, Phatumthani 12121, Thailand

post-surface treatment methods providing MSNPs functionalized with methyl groups [17, 30–34]. Heat treatment and spray-drying are other reported techniques generating rough morphologies to improve hydrophobicity of the MSNPs as well, yet, they required sophisticated instrument [35, 36]. However, from those literatures, the shape and pore structure inside the particles were not well controlled and the water contact angle was not reported.

Here in, we report the one-pot synthesis of core—shell MSNPs with a well-control in shape, size, and pore structure using a facile method. The effects of ethanol on the particle size and the concentration of fluoroalkyl silane on surface wettability were thoroughly investigated. An assembly of the MSNPs with nanostructured surface roughness on the substrate generated a dual morphology with low surface energy providing oleophobic and ultrahydrophobic properties. The MSNPs prepared from this method show a potential that can be applied in coating applications.

### 2 Experimental

#### 2.1 Chemicals

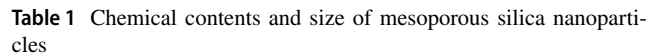
Tetraethyl orthosilicate 99% (TEOS), trimethyl(fluoromethyl) silane 99% (F<sub>3</sub>-silane), and trichloro(*1H*, *1H*, *2H*, *2H*-perfluorooctyl)silane 97% (F<sub>13</sub>-silane) were purchased from Sigma-Aldrich. Ammonia solution 25% (NH<sub>4</sub>OH) was purchased from EMSURE®. *N*-Cetyl-*n*, *n*, *n* trimethyl ammonium bromide (CTAB) was purchased from Loba Chemie. Absolute ethanol anhydrous 99% (EtOH) was purchased from RCI Labscan. All chemicals were used as received.

### 2.2 Synthesis of MSNPs

First, 0.6 g of CTAB was dissolved in 150 mL of water in a three-necked round bottom flask. The solution was stirred and heated at 60 °C for 30 min. To the solution, 50 mL of EtOH and 15 mL of NH<sub>4</sub>OH were added subsequently. Then, 6 mL of TEOS was added dropwise under vigorous stirring. The amount of H<sub>2</sub>O and EtOH of each condition is shown in Table 1. The reaction mixture was stirred at 60 °C under nitrogen atmosphere for 6 h and then cooled to room temperature. The MSNPs were collected by centrifugation (LD-3, 2000 rpm), washed with water followed by EtOH, and oven-dried at 60 °C. The MSNPs were stored in a desiccator before further studies.

### 2.3 Synthesis of MSNPs functionalized with fluoroalkyl silane (F<sub>x</sub>-MSNPs)

Similar method used to synthesize MSNPs as described above was carried. Subsequently, after adding half of



Sample	Water (mL)	EtOH (mL)	TEOS:F- silane	Size (nm)
MSNP-1	190	0	_	176±20
MSNP-2	180	20	_	$201 \pm 23$
MSNP-3	170	30	_	$270 \pm 34$
MSNP-4	160	40	_	$279 \pm 28$
MSNP-5	150	50	_	$568 \pm 24$
MSNP- F <sub>3</sub> -20,1	160	40	20:1	$287 \pm 22$
MSNP- F <sub>3</sub> -10,1	160	40	10:1	$291 \pm 18$
MSNP-F <sub>3</sub> -5,1	160	40	5:1	$298 \pm 27$
MSNP- F <sub>13</sub> -20,1	160	40	20:1	$290 \pm 22$
MSNP- F <sub>13</sub> -10,1	160	40	10:1	$317 \pm 24$
MSNP- F <sub>13</sub> -5,1	160	40	5:1	$368 \pm 56$

TEOS, F<sub>x</sub>-silane was added simultaneously to the solution. The MSNPs were collected by centrifugation, washed with water followed by EtOH, and oven-dried at 60 °C. The MSNPs were stored in a desiccator before further studies.

#### 2.4 Characterization

Particle size and morphology of the MSNPs were determined by scanning electron microscopy (SEM, FEI Quanta-400 and FESEM, Merlin compact, Zeiss). The surface of the samples was coated with a thin layer of gold before an examination. SEM equipped with an energydispersive X-ray spectrometer (EDS) was used to study chemical compositions on the surface of the MSNPs. The average size of the MSNPs was measured by using Image J software and calculated from the sizes of 100 MSNPs in SEM images. Pore structure of the MSNPs was studied by transmission electron microscopy (TEM, JEOL JEM-2010) using an accelerating voltage of 200 kV. The N<sub>2</sub> adsorption/desorption isotherms were measured with Quantachrome Autosorb 1MP. The samples were outgassed at 80 °C for 4 h. The surface area was calculated by using Brunauer-Emmett-Teller (BET) method and the pore size was obtained from Barrett-Joyner-Halenda (BJH) method. Thermal stability of the MSNPs was characterized by simultaneous thermogravimetric analyzer (STA, PERKIN STA-8000) in air, from 25 to 900 °C with the heating rate of 10 °C/min. Contact angles of the surface coated with the MSNPs were measured by VCA optima goniometer system.



### 3 Results and discussion

### 3.1 The effect of a cosolvent on the size and the pore structure of the MSNPs

The MSNPs were synthesized successfully using CTAB as a template and EtOH as a cosolvent. Figure 1 shows the SEM micrographs of the MSNPs with smooth surface synthesized from various ratios of  $\rm H_2O$ :EtOH. The shape of the MSNPs obtained from each condition is spherical-like with narrow size distribution. Similar shape of particle was also obtained when octadecyltrimethylammonium chloride was used as a template [37]. The spherical shape of particle is generated due to the low surface tension of

micelles induced by EtOH in the system [18]. The proposed mechanism for the formation of MSNPs via surfactant template with an addition of cosolvent is illustrated in Scheme 1. At the beginning, CTAB molecules formed micelles and silica oligomers were absorbed on the surface of the micelles. An attractive force between micelles induced aggregation of micelles followed by condensation of the silica oligomers. Finally, silica polymers were obtained having CTAB micelles as reservoirs [38–40].

The size of the prepared MSNPs was analyzed using Image J software and the results were shown in Table 1. It can be seen that an increase in the amount of EtOH from 0 to 50 mL led to a significant increase of the diameter of the MSNPs from  $176 \pm 20$  to  $568 \pm 24$  nm. The results are consistent with the study of Yano et al. and Teng et al. reporting

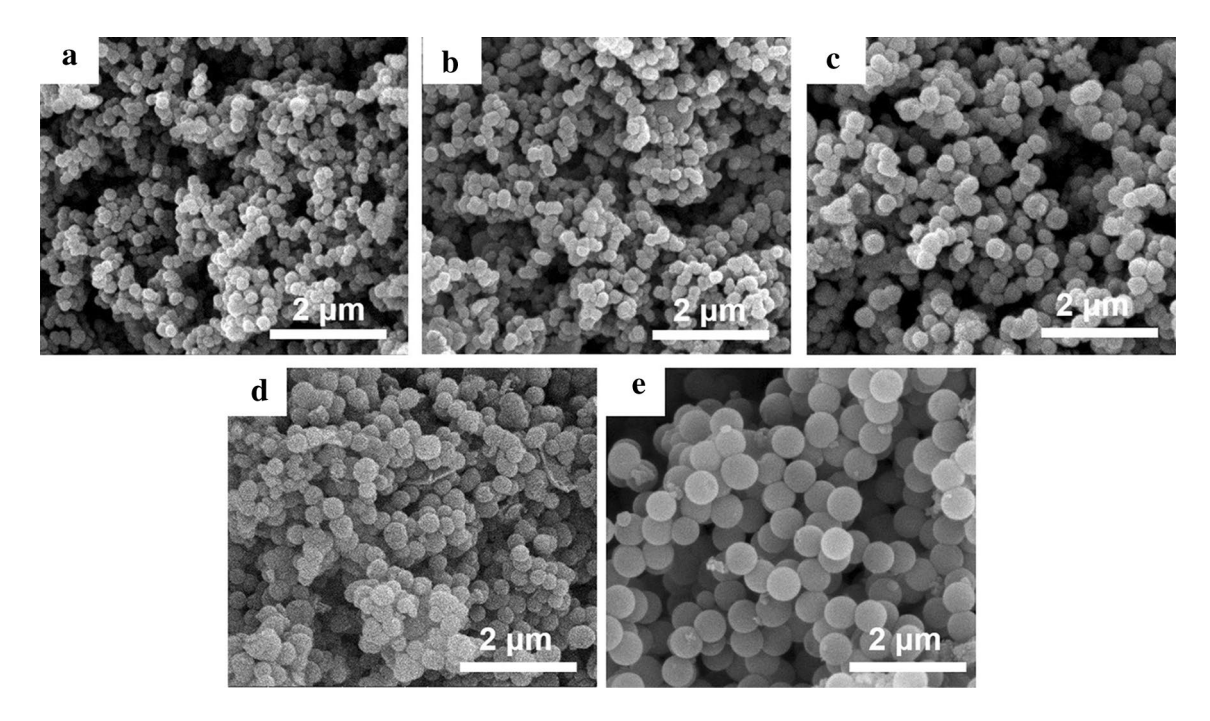
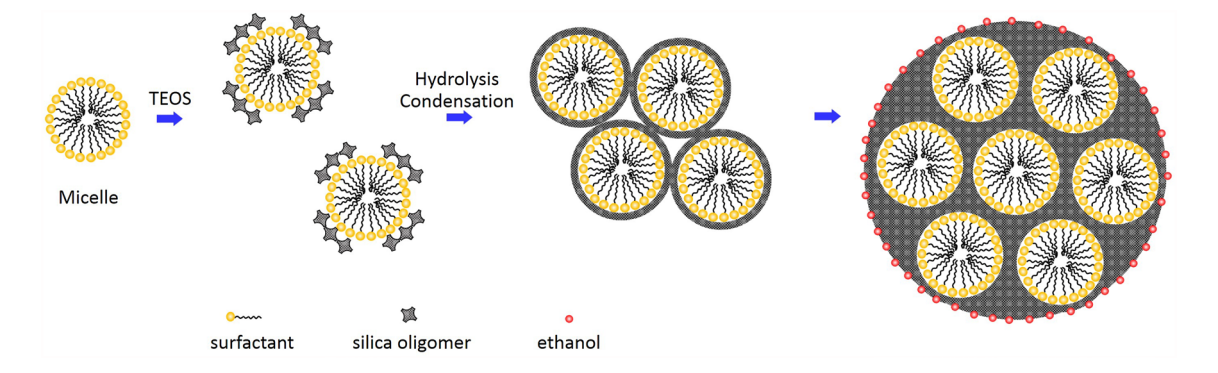


Fig. 1 SEM micrographs of mesoporous silica nanoparticles synthesized with different  $H_2O$ :EtOH volume ratios **a** 190:0, **b** 180:20, **c** 170:30, **d** 160:40, and **e** 150:50



Scheme 1 The proposed mechanism for the formation of the mesoporous silica nanoparticles

an increase of particle size of the MSNPs containing ordered hexagonal pores [16, 41]. The growth of the particle size was due to a slow process of hydrolysis and condensation of silica precursors at high concentration of EtOH. A slow nucleation and an increase in precipitation time of silica led to an increase in the MSNP diameter [6, 41]. Besides, EtOH would penetrate into microemulsion droplets and enlarge the size of the MSNPs [42]. The results indicate that the cosolvent system can be used as an alternative method to control the size of the MSNPs.

TEM was used to confirm the pores inside and on the surface of the MSNPs. Figure 2 reveals two different pore structures inside the MSNPs obtained from different H<sub>2</sub>O:EtOH volume ratios. Using CTAB as a surfactant template was reported to generate hexagonal pores inside the particles [18, 43, 44]. Nevertheless, from our study it can be seen that at low concentration of EtOH, the pores inside the MSNPs assembled in a lamellar structure, Fig. 2a, b with the spacing ~ 5 nm. At higher EtOH concentration, however, the pore structure transformed to radial-like structure from the center to the surface of the particle, Fig. 2c-e. These results are in agreement with those of Wu et al. in which they found that lamellar CTAB micelles formed at low concentration of EtOH and further addition of EtOH led to the transformation to spherical micelles [45]. This indicated that not only the type of surfactant template showed an important role in controlling the pore structure but also the concentration of the cosolvent. Alternating of pore structure was also reported when polar, protic, and aprotic solvents were used as cosolvents [46, 47]. Note that the shape of the MSNPs is an irregular sphere with some elliptical MSNPs at low concentration of EtOH. The reason is owing to the fact that the surfactant molecules form cylindrical structure in the dilute system of CTAB [7]. Although EtOH has high surface tension (72 mJ/m²), low amount of EtOH was not adequate to reduce surface tension of micelles and induce spherical shape. Thus, the elliptical MSNPs were obtained as a mixture [18].

#### 3.2 Surface functionalization of the MSNPs

The surface of the MSNPs was covered with hydroxyl groups that imparted hydrophilic characteristic. In order to increase hydrophobicity and oleophobicity on the surface of the MSNPs for the purpose of coating application, the surface of the particles was functionalized with fluoroalkyl silanes that are well known to provide very low surface energy, less than 20 mJ/m² [48, 49]. Since the MSNP-4 system rendered spherical nanoparticles with narrow size distribution, the system was selected for further study. Figure 3 reveals TEM micrographs of the MSNPs functionalized with F<sub>3</sub>-silane at different concentrations. It is observed that a subsequent

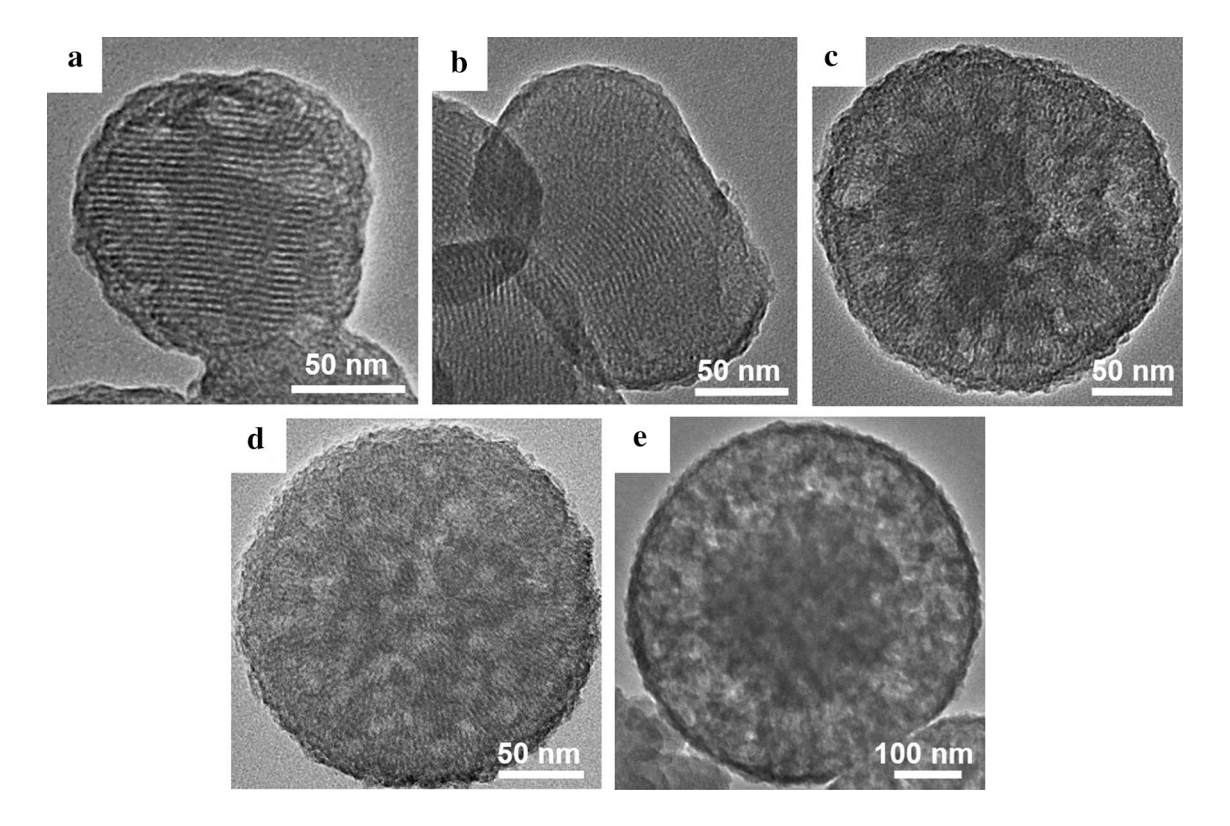


Fig. 2 TEM micrographs of mesoporous silica nanoparticles synthesized with different H<sub>2</sub>O:EtOH volume ratios **a** 190:0, **b** 180:20, **c** 170:30, **d** 160:40, and **e** 150:50



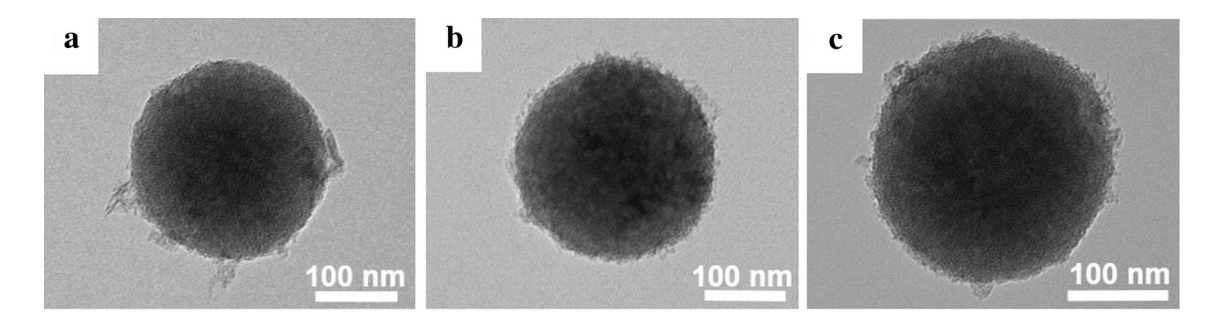


Fig. 3 TEM images of fluorinated mesoporous silica nanoparticles with varied TEOS:F<sub>2</sub>-silane mole ratios a 20:1, b 10:1, and c 5:1

addition of  $F_3$ -silane generated a core–shell structure composing MSNP as a core and hair-like layer around the particle as a shell. Increasing the mole ratio of  $F_3$ -silane from TEOS: $F_3$ -silane of 20:1 to 5:1 led to an increase in the shell coverage as evidenced in TEM images. In addition, the sizes of the  $F_3$ -MSNPs slightly increased (287  $\pm$  22, 291  $\pm$  18, and 298  $\pm$  27 nm, respectively) compared to that of MSNP-4 (279  $\pm$  28 nm).

Due to the fact that surface free energies of fluorinated compounds vary with chemical structure and length of fluoroalkyl chain [50], the MSNPs were functionalized with longer fluoroalkyl chain to increase hydrophobicity of the particles. Figure 4 shows TEM micrographs and SEM-EDS spectroscopic mapping of the MSNPs functionalized with F<sub>13</sub>-silane at different concentrations. TEM images of the MSNPs exhibit a similar trend of the results mentioned previously. Moreover, it is obvious that an increase in F<sub>13</sub>-silane concentration led to an increase in thickness and density of the shell and the F<sub>13</sub>-silane yielded a thicker hair-like layer around the MSNPs compared to F<sub>3</sub>-silane. This can be attributed to an increase in the length of fluoroalkyl chain [51]. Surface functionalization with F-silane was also confirmed by SEM-EDS. The EDS mappings of MSNP-F<sub>13</sub>-20,1, MSNP-F<sub>13</sub>-10,1, and MSNP-F<sub>13</sub>-5,1 reveal uniform distribution of fluorine on the surface of the MSNPs and the F/Si atomic ratios increased with the increment of TEOS: $F_{13}$ -silane from 0.10 to 1.06 and 1.20, respectively. These results are consistent with TEM images that show core-shell structure of the particles.

High resolution SEM images of the MSNP-4, MSNP- $F_3$ -5,1, and MSNP- $F_{13}$ -5,1 are shown in Fig. 5. Before surface functionalization, pores can be clearly observed on the surface of MSNP-4, Fig. 5a. After surface functionalization with F-silane, the size of MSNP- $F_3$ -5,1 and MSNP- $F_{13}$ -5,1 changed significantly to  $298 \pm 27$  and  $368 \pm 56$  nm, respectively. In addition, the morphology of the particles changed from smooth surface to very rough surface as shown in Fig. 5b, c due to the coating of long fluoroalkyl chain that generated nanostructure surface roughness [52, 53]. It should be noted that small particles were not observed

in the SEM images indicating that the number of nucleation site had been fixed since the early step of hydrolysis and condensation of TEOS and the F-silane only reacted on the surface of the nucleating particles [7, 39]. This is consistent with the result of LaMer method in which monomeric silica would coat on the nucleating sites when low concentration of silane is added [39, 54].

Figure 6a shows adsorption/desorption isotherms of the MSNPs with lamellar pore structure and radial-like pore structure before and after surface functionalization with F-silane. It can be seen that all samples exhibited a typical type IV curves which was a characteristic of mesoporous materials. Although it was reported that co-condensation with long fluorocarbon would affect to pores on the surface and reduce porous order [17], our results suggested that surface functionalization by co-condensation with F-silane did not affect porous structure. BET specific surface area were about 284 m<sup>2</sup>/g for lamellar-pore MSNPs and about 728-779 m<sup>2</sup>/g for radial-pore MSNPs. The pore radius of the MSNPs was about 54 Å for lamellar-pore MSNPs and in the range of 20-22 Å for radial-pore MSNPs indicating very narrow mesoporous nanoparticles. The pore size calculated from BJH analysis was consistent with the pore size measured from TEM images.

### 3.3 The effect of surface functionalization on thermal stability of the MSNPs

Thermal stabilities of the MSNPs with and without surface functionalization are shown in Fig. 7. All samples display three major regions of weight-loss. The first region manifested a weight loss of 1.3–5.2 wt% between 25 and 230 °C, attributed to the loss of moisture and the desorption of absorbed water in the pores of the MSNPs [55, 56]. The second region between 190 and 308 °C exhibited a weight loss of 9.4–19.4 wt% corresponded to the loss of residual CTAB inside the pores of the MSNPs and dihydroxylation of silanol [51]. The third region showed the significant weight loss of 4.9–34.0 wt% between 300 and 511 °C corresponded to the loss of residual remaining organic fragments



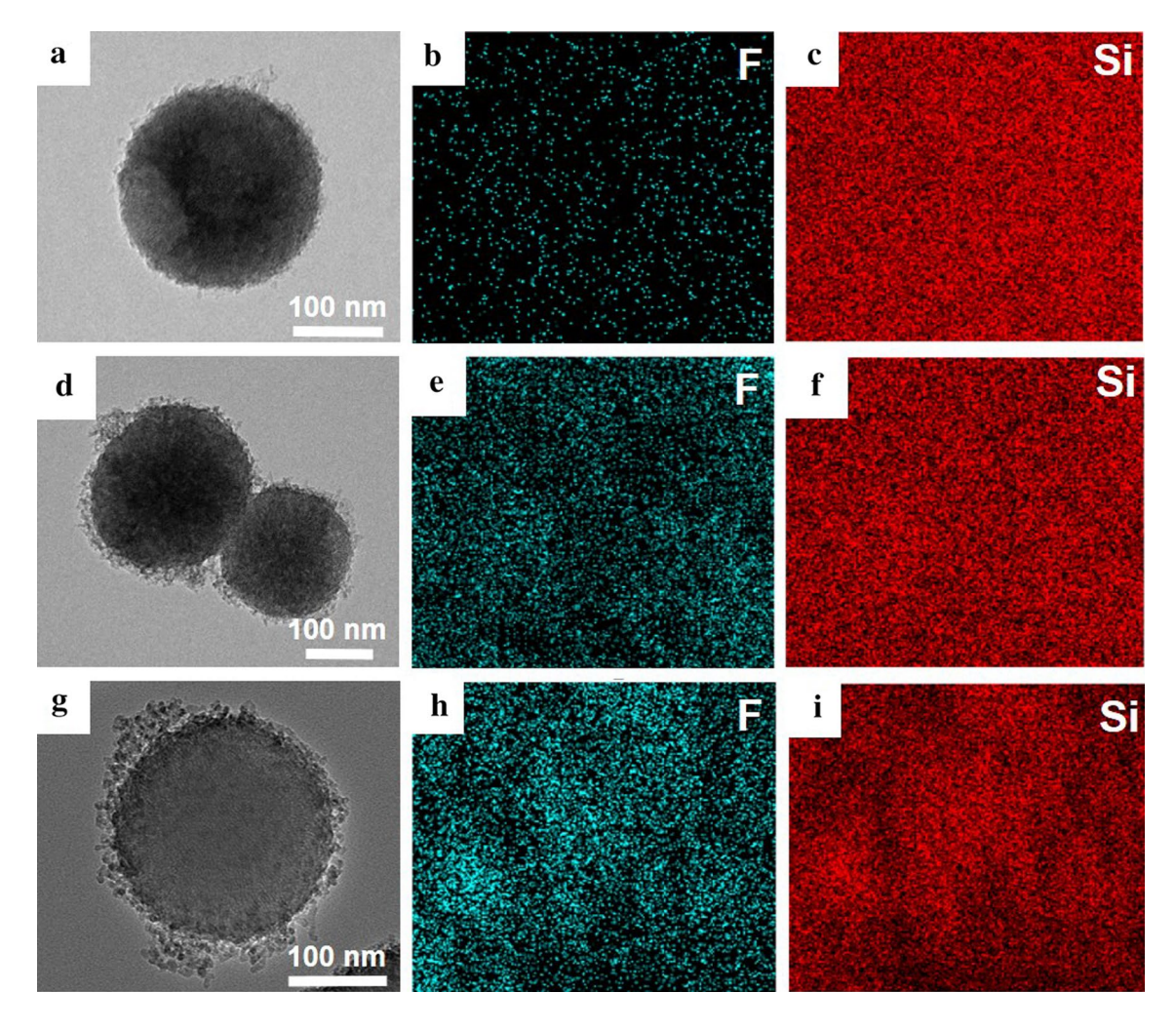


Fig. 4 TEM images and SEM-EDS spectroscopic mapping of fluorinated mesoporous silica nanoparticles with varied TEOS: $F_{13}$ -silane mole ratios  $\mathbf{a}$ - $\mathbf{c}$  20:1,  $\mathbf{d}$ - $\mathbf{f}$  10:1, and  $\mathbf{g}$ - $\mathbf{i}$  5:1

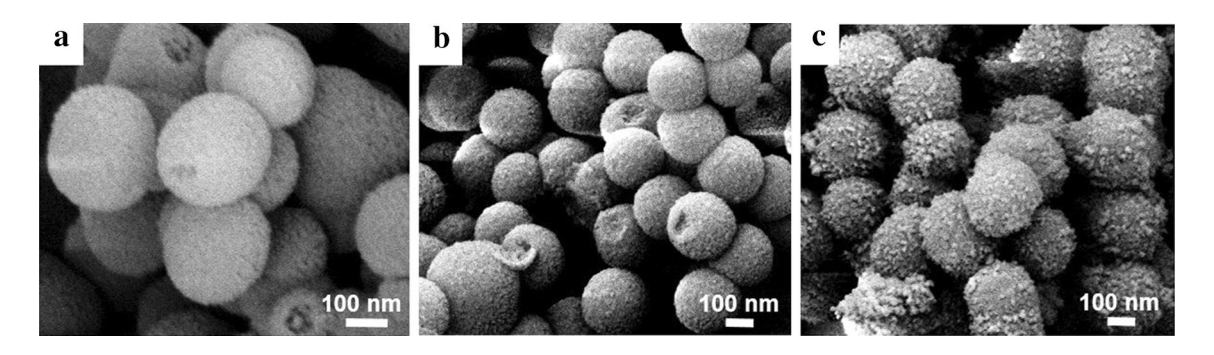


Fig. 5 High resolution SEM images of a MSNP-4, b MSNP-F<sub>3</sub>-5,1, and c MSNP-F<sub>13</sub>-5,1

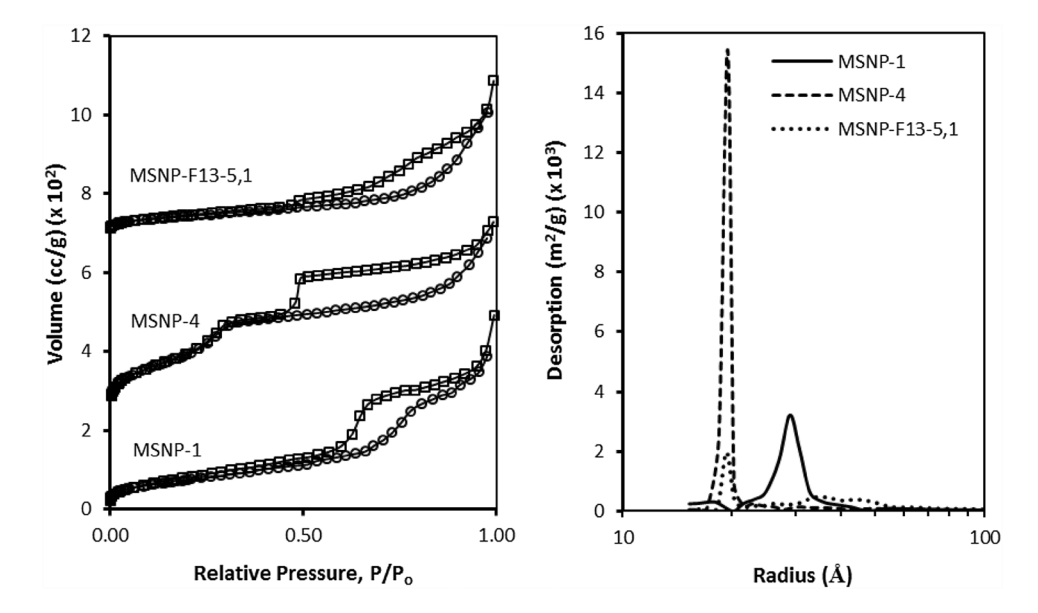
and decomposition of fluoroalkyl fragments [17]. Moreover, it can be seen that the MSNPs functionalized with  $F_{13}$  showed higher thermal stability compared to the MSNPs without surface functionalization. Furthermore, the sample with higher concentration of  $F_{13}$ , i.e. MSNP- $F_{13}$ -5,1, showed higher degradation temperatures and % weight loss than

those of lower concentration of  $F_{13}$ , MSNP- $F_{13}$ -10,1 and MSNP- $F_{13}$ -20,1, respectively. This is attributed to surface coating with fluoro-silica [57].

The percent weight loss in the temperature range of 300–511 °C of MSNP- $F_{13}$ -20,1, MSNP- $F_{13}$ -10,1, and MSNP- $F_{13}$ -5,1 were 15.4, 17.0, and 34.0 wt%, respectively.



**Fig. 6** Nitrogen adsorption—desorption isotherms (**a**) (offset vertically by 200 and 700 for MSNP-4 and MSNP-F<sub>13</sub>-5,1, respectively) and BJH pore size distribution curves (**b**) of MSNPs



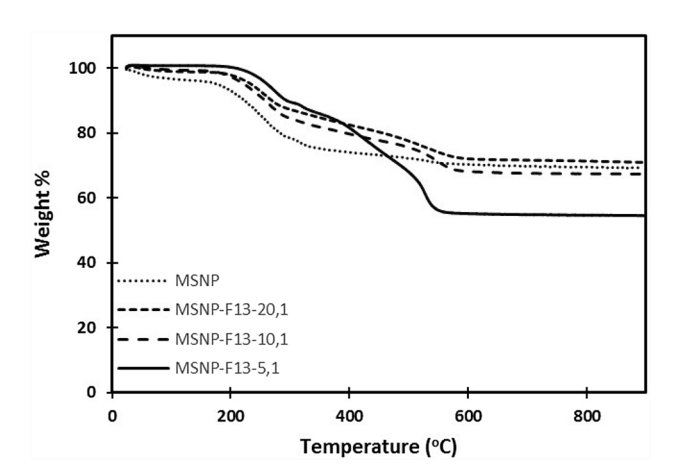


Fig. 7 TGA thermograms of mesoporous silica nanoparticles

These results indicated that the amount of weight loss in the last region correlated with the mole ratio of F-silane loading as well. The results are consistent with the work of Compos et al. that the weight loss of fluoroalkyl chain functionalized fumed silica and precipitate silica increased with an increase of fluoroalkyl silane loading [51].

### 3.4 The effect of surface functionalization on surface wettability of the MSNPs

Water contact angles (CAs) of a glass substrate coated with the MSNPs and photographs of a water droplet on the substrate were shown in Table 2 and Fig. 8, respectively. It is obvious that the coated substrate with fluoroalkyl functionalized MSNPs improved hydrophobicity of the substrate in such a way that the water CAs, both advancing CA and receding CA, increased significantly. Increasing mole

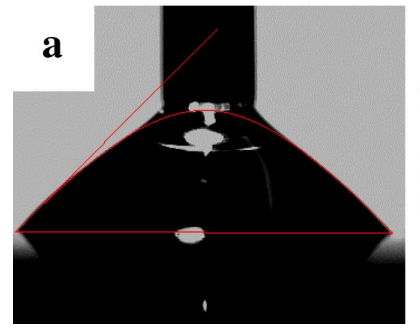
**Table 2** Water contact angles of glass substrates coated with mesoporous silica nanoparticles

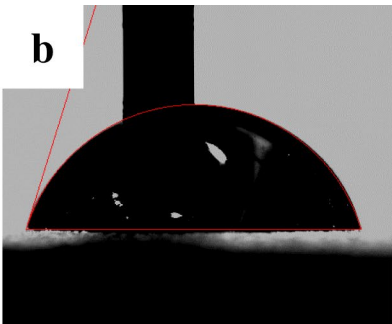
Sample	Advancing (°)	Receding (°)	
MSNP-4	46.3	24.1	
MSNP-F <sub>3</sub> -20,1	60.8	20.9	
MSNP-F <sub>3</sub> -10,1	66.3	26.5	
MSNP-F <sub>3</sub> -5,1	68.9	23.8	
MSNP-F <sub>13</sub> -20,1	92.4	40.8	
MSNP-F <sub>13</sub> -10,1	126.5	33.7	
MSNP-F <sub>13</sub> -5,1	152.7	73.7	

ratio of F-silane tends to increase CAs of the substrates. Moreover, the MSNPs functionalized with long fluoroalkyl chain,  $F_{13}$ -silane, resulted in much higher CAs (100–230% increase) compared to those of shorter fluoroalkyl chain,  $F_{3}$ -silane (31–49% increase). MSNP- $F_{13}$ -5,1 imparted average advancing CA of 152.7° with the highest value of 158.6° which is a characteristic of super-hydrophobic and oleophobic material [58]. These results were consistent with the morphology of the MSNPs as shown in TEM images that the fluoroalkyl shell was thicker when the surface of the MSNPs was functionalized with  $F_{13}$ -silane.

It was reported previously that fluoro-treated smooth surfaces provided CA not higher than 125° [58]. Gao et al. reported that the substrate coated with very small silica nanoparticles (80 nm) functionalized with acyl fluoride perfluoropolyether ( $C_9F_{18}O_3$ ) provided a static water CA of 151.4° [59]. Although the size of the MSNPs synthesized from our method was larger with shorter fluoroalkyl silane, the resulted water CA was higher. This should be attributed to the greater surface roughness of the MSNPs as evidenced by HR–SEM images. Thus, it can be concluded







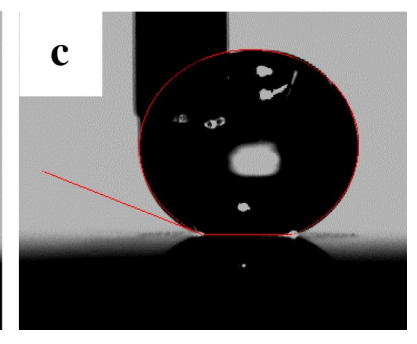


Fig. 8 Photographs of water droplets on glass substrates coated with mesoporous silica nanoparticles; a MSNP-4, b MSNP- $F_3$ -5,1, c MSNP- $F_{13}$ -5,1

that a remarkably ultrahydrophobic and oleophobic properties of the MSNP- $F_{13}$  is strongly influenced by the porosity and the roughness of the MSNP surface [52, 53]. This rough texture generated nano-voids for air trapping underneath a water droplet preventing water to form a full contact with the surface as described by Cassie–Baxter's theory that assumed the resting of liquid on the peaks of the rough structure [60–62].

#### 4 Conclusions

The spherical MSNPs with narrow size distribution were synthesized successfully using CTAB as a cationic surfactant template and EtOH as a cosolvent. Increasing volume ratio of EtOH resulted in both an enlargement of the particles and changing pore structure inside the particles from a lamellar structure to a radially oriented structure. Surface wettability of the MSNPs was improved by functionalization with two different types of fluoroalkyl silane. The MSNPs formed a core-shell structure after co-condensation with F-silane. Increasing mole ratio of F-silane generated thick and dense hair-like shell, thus, the morphology of the particles changed from smooth surface to very rough surface. Water CA measurement proved that hydrophobicity and oleophobicity of the particles were improved significantly from 46.3° to 158.6° after the chemical modification with  $F_{13}$ -silane. Finally, the MSNPs prepared by this method provided ultrahydrophobic property from a combination of surface chemistry and nanostructured surface roughness. Therefore, they show potentiality to be used in coating applications.

**Acknowledgements** This work was financially supported by the Thailand Research Fund (TRF) (Grant Number TRG5880154) and the Prince of Songkla University (PSU), Thailand. The funding sources had no involvement in the discussion in this report.

### **Compliance with ethical standards**

Conflict of interest The authors declare that they have no conflict of interest.

### References

- F. Iskandar, I.W. Lenggoro, T.O. Kim, N. Nakao, M. Shimada, K. Okuyama, J. Chem. Eng. Jpn. 34, 1285 (2001)
- A. Liberman, N. Mendez, W.C. Trogler, A.C. Kummel, Surf. Sci. Rep. 69, 132 (2014)
- C.T. Kresge, M.E. Leonowicz, W.J. Roth, J.C. Vartuli, J.S. Beck, Nature 359, 710 (1992)
- J.S. Beck, J.C. Vartuli, W.J. Roth, M.E. Leonowicz, C.T. Kresge, K.D. Schmitt, C.T.W. Chu, D.H. Olson, E.W. Sheppard, S.B. McCullen, J.B. Higgins, J.L. Schlenker, J. Am. Chem. Soc. 114, 10834 (1992)
- Z. Mao, L. Hu, Q. Zhao, C. Gao, Chem. Res. Chin. Univ. 28, 546 (2012)
- 6. K. Yano, Y. Fukushima, J. Mater. Chem. 13, 2577 (2003)
- R.I. Nooney, D. Thirunavukkarasu, Y. Chen, R. Josephs, A.E. Ostafin, Chem. Mater. 14, 4721 (2002)
- 8. G. Büchel, M. Grün, K.K. Unger, A. Matsumoto, T. Kazuo, Supramol. Sci. 5, 253 (1998)
- 9. D. Zhao, J. Feng, Q. Huo, N. Melosh, G.H. Fredrickson, B.F. Chmelka, G.D. Stucky, Science **279**, 548 (1998)
- A.B.D. Nandiyanto, S.-G. Kim, F. Iskandar, K. Okuyama, Microporous Mesoporous Mater. 120, 447 (2009)
- 11. F. Iskandar, K. Okuyama, Nano Lett. 2, 389 (2002)
- J. Rathousky, M. Zukalova, P.J. Kooyman, A. Zukal, Colloids Surfaces A 241, 81 (2004)
- C.J. Brinker, Y. Lu, H. Fan, A. Stump, T.L. Ward, T. Rieker, Nature 398, 223 (1999)
- J. Yu, J.-L. Shi, H.-R. Chen, J.-N. Yan, D.-S. Yan, Microporous Mesoporous Mater. 46, 153 (2001)
- H. Qisheng, D.I. Margolese, G.D. Stucky, Chem. Mater. 8, 1147 (1996)
- 16. K. Yano, Y. Fukushima, J. Mater. Chem. 14, 1579 (2004)
- C. Pereira, C. Alves, A. Monteiro, C. Magén, A.M. Pereira, A. Ibarra, M.R. Ibarra, P.B. Tavares, J.P. Araújo, G. Blanco, J.M. Pintado, A.P. Carvalho, J. Pires, M.F.R. Pereira, C. Freire, ACS Appl. Mater. Interfaces 3, 2289 (2011)
- J. Domínguez, E. Terrés, A. Vázquez, Microporous Mesoporous Mater. 66, 341 (2003)



- Q. Chen, L. Han, C. Gao, S. Che, Microporous Mesoporous Mater. 128, 203 (2010)
- 20. K. Möller, J. Kobler, T. Bein, Adv. Funct. Mater. 17, 605 (2007)
- M. Grün, I. Lauer, K.K. Unger, M. Grün, I. Lauer, K.K. Unger, Adv. Mater. 9, 254 (1997)
- K. Benson, E.A. Prasetyanto, H.-J. Galla, N.S. Kehr, S.S. Park, C.S. Ha, I. Lopez-Duarte, M.V.M. Díaz, H. Kessler, B. Geiger, J.P. Spatz, Soft Matter 8, 10845 (2012)
- 23. F. Tang, L. Li, D. Chen, Adv. Mater. 24, 1504 (2012)
- X. Mei, D. Chen, N. Li, Q. Xu, J. Ge, H. Li, B. Yang, Y. Xu, J. Lu, Soft Matter 8, 5309 (2012)
- K. Unger, D. Kumar, M. Grün, G. Büchel, S. Lüdtke, T. Adam, K. Schumacher, S. Renker, J. Chromatogr. A 892, 47 (2000)
- A. Kurganov, K. Unger, T. Issaeva, J. Chromatogr. A 753, 177 (1996)
- T. Nassivera, A.G. Eklund, C.C. Landry, J. Chromatogr. A 973, 97 (2002)
- J.L. Vivero-Escoto, I.I. Slowing, B.G. Trewyn, V.S.-Y. Lin, Small 6, 1952 (2010)
- 29. N.K. Mal, M. Fujiwara, Y. Tanaka, Nature 421, 350 (2003)
- D. Yang, Y. Xu, D. Wu, Y. Sun, H. Zhu, F. Deng, J. Phys. Chem. C 111, 999 (2006)
- 31. Y. Zhao, J. Song, D. Wu, T. Tang, Y. Sun, J. Phys. Chem. Solids **86**, 1 (2015)
- Y. Zhao, D. Wu, T. Tang, Y. Sun, Mater. Res. Bull. 48, 4839 (2013)
- 33. H. Gu, H.F. Ji, Y.L. Deng, R.J. Dai, Mater. Technol. 29, 21 (2014)
- 34. G. Zhao, Z. Zhao, J. Wu, D. Ye, J. Spectrosc. 2014, 965037 (2014)
- 35. Y.J. Cao, Z.F. Wu, Adv. Mater. Res. **152–153**, 856 (2010)
- P.B. Sarawade, J.-K. Kim, A. Hilonga, H.T. Kim, Powder Technol. 197, 288 (2010)
- K. Yano, M.B. Katz, X. Pan, N. Tatsuda, J. Colloid Interface Sci. 418, 61 (2014)
- Z. Yi, L.F. Dumée, C.J. Garvey, C. Feng, F. She, J.E. Rookes, S. Mudie, D.M. Cahill, L. Kong, Langmuir 31, 8478 (2015)
- J. Frasch, B. Lebeau, M. Soulard, J. Patarin, R. Zana, Langmuir 16, 9049 (2000)
- K. Flodström, H. Wennerström, V. Alfredsson, Langmuir 20, 680 (2003)
- Z. Teng, X. Su, B. Lee, C. Huang, Y. Liu, S. Wang, J. Wu, P. Xu,
   J. Sun, D. Shen, W. Li, G. Lu, Chem. Mater. 26, 5980 (2014)

- 42. W. Yang, B. Li, Nanoscale 6, 2292 (2014)
- Q. Cai, W.-Y. Lin, F.-S. Xiao, W.-Q. Pang, X.-H. Chen, B.-S. Zou, Microporous Mesoporous Mater. 32, 1 (1999)
- Q. Cai, Z.-S. Luo, W.-Q. Pang, Y.-W. Fan, X.-H. Chen, C. Fu-Zhai, Chem. Mater. 13, 258 (2001)
- L. Wu, Z. Jiao, M. Wu, T. Song, H. Zhang, RSC Adv. 6, 13303 (2016)
- M.T. Anderson, J.E. Martin, J.G. Odinek, P.P. Newcomer, Chem. Mater. 10, 311 (1998)
- M. Grün, K.U. Klaus, A. Matsumoto, T. Kazuo, Microporous Mesoporous Mater. 27, 207 (1999)
- A. Yildirim, H. Budunoglu, B. Daglar, H. Deniz, M. Bayindir, ACS Appl. Mater. Interfaces 3, 1804 (2011)
- 49. J.-D. Brassard, D.K. Sarkar, J. Perron, Appl. Sci. **2**, 453 (2012)
- T. Nishino, M. Meguro, K. Nakamae, Int. J. Adhes. Adhes. 19, 399 (1999)
- R. Campos, A.J. Guenthner, T.S. Haddad, J.M. Mabry, Langmuir 27, 10206 (2011)
- S.M.M. Ramos, A. Benyagoub, B. Canut, C. Jamois, Langmuir 26, 5141 (2010)
- S.R. Coulson, I. Woodward, J.P.S. Badyal, S.A. Brewer, C. Willis, J. Phys. Chem. B **104**, 8836 (2000)
- 54. V.K. LaMer, R.H. Dinegar, J. Am. Chem. Soc. 72, 4847 (1950)
- G. Osei-Prempeh, H.-J. Lehmler, A.-F. Miller, B.L. Knutson, S.E. Rankin, Microporous Mesoporous Mater. 129, 189 (2010)
- 56. J. Kecht, T. Bein, Microporous Mesoporous Mater. 116, 123 (2008)
- Z. Ye, Y. Chen, X. Yang, W. Hu, H. Ye, Colloids Surfaces A 514, 251 (2017)
- L.Y.L. Wu, S.K. Ngian, Z. Chen, D.T.T. Xuan, Appl. Surf. Sci. 257, 2965 (2011)
- Y. Gao, Y. Huang, S. Feng, G. Gu, F.-L. Qing, J. Mater. Sci. 45, 460 (2010)
- 60. A.B.D. Cassie, S. Baxter, Trans. Faraday Soc. 40, 546 (1944)
- C.-T. Hsieh, W.-Y. Chen, F.-L. Wu, Y.-S. Shen, J. Adhes. Sci. Technol. 22, 265 (2008)
- K. Tadanaga, N. Katata, T. Minami, J. Am. Ceram. Soc. 80, 3213 (1997)

